Author's response by Wenjie Wang et al.

Corresponding to mshao@pku.edu.cn.

We greatly appreciate the time and efforts that the Referees spent in reviewing our manuscript. The comments are really thoughtful and helpful to improve the quality of our paper. We have addressed each comment below, with the Referee comment in black text, our response in blue text, and relevant manuscript changes noted in red text.

Anonymous Referee #1

Line 30: "In addition, the slopes are equal to ...." 1) The wording: "In addition, ..." is awkward. 2) Why there is a range of slopes for j(O^1D) and a single value for j(NO2) is

unclear at this point, and what the slopes refer to in the first place when the relationships are non-linear. 3) The slopes should be negative in any case. 4) The authors should take into account significant digits (throughout the paper). The precision of the data does not justify a statement "4.21-6.93". I would say "4.2-6.9" at the very most. 5)

AOD has to be specified here, i.e. AOD (380 nm)?

Response: 1) I have removed the phrase "In addition".

2) There is a range of slopes for j(O^1D) is because that the slopes varied at different total ozone column. Table 3 gives different slopes for j(O^1D) at different ozone column classes. For j(NO_2), total ozone column has a negligible influence on the slope. The slopes are at AOD smaller than 0.7, where the relationship between j-value and AOD is close to linear. We chose this range of AOD (AOD<0.7) to match the result in Crete by Gerasopoulos et al. (2012).

3) Yes, the slopes should be negative in any case. Therefore, in Line 30, I changed "the slopes" into "the absolute values of slopes".

4) Many thanks and I have taken into account significant digits throughout the paper.

5) I have added AOD (380 nm) in line27.

Line 27: Both j(O^1D) and j(NO_2) display significant dependence on AOD (380nm) with a nonlinear negative correlation.

Line 30-34: The absolute values of slopes are equal to 4.2-6.9▪10^{-6} s^{-1} and 3.2▪10^{-3} s^{-1} per AOD unit for j(O^1D) and j(NO_2) respectively at SZA of 60° and AOD smaller than 0.7, both of which are larger than those observed in a similar, previous study in the Mediterranean.

Line 32: "... larger than those observed in the Mediterranean." I would say: "... than those observed in a similar, previous study in the Mediterranean."

Response: Thank you and I have revised it in the manuscript.

Line 30-34:The absolute values of slopes are equal to 4.2-6.9▪10^{-6} s^{-1} and 3.2▪10^{-3} s^{-1}per AOD unit for j(O^1D) and j(NO_2) respectively at SZA of 60° and AOD smaller than 0.7, both of which are larger than those observed in a similar, previous study in the Mediterranean.

Line 33: "...have a stronger extinction on ..." Please reword.

Response: I have changed it into "...have a stronger extinction effect on ...".

Line 34-36: This indicates that the aerosols in urban Beijing have a stronger extinction effect on actinic flux than absorptive dust aerosols in the Mediterranean.

Line 38, 39: "... j(NO2) by 24.2% and 30.4% for summer and winter, ... j(O1D) by 27.3% and 32.6%..." 1) The meaning of these numbers is unclear. I assume they refer to some kind of seasonal mean of the photolysis frequencies that needs to be specified. 2) The precision implied by three digits is misleading.

Response: Thank you and I have revised it. We calculated the reduction ratios of j values in the following procedure: We use the parametric equations (Table 5 and Table

6) to calculated J(O1D) and J(NO2) using corresponding SZA, AOD and ozone column at corresponding time (5 minute average). Two situations are calculated: One, AOD is equal to 0 at all times. Two, AOD is equal to the observed values at all times. The mean values of J(O1D) and J(NO2) for summer and winter are calculated in the two situations and the reduction ratios can be calculated accordingly.

Line 39-42: According to the parametric equation, aerosols lead to a decrease in seasonal mean j(NO_2) by 24% and 30% for summer and winter, respectively, and the corresponding decrease in seasonal mean j(O^1D) by 27% and 33% respectively, compared to an aerosol-free atmosphere (AOD = 0).

Line 42: "... the monthly average net ozone production is reduced by 25%." By looking

at Fig. 10, I assume the 25% refers to a monthly mean daytime net ozone production that needs to be specified.

Response: Yes, the 25% refers to a monthly mean daytime net ozone production. I have specified it.

Line 44: The simulation results shows that the monthly mean daytime net ozone production rate is reduced by up to 25% due to the light extinction of aerosols.

Lines 54, 59, 63, 65, 66: Use consistent notations for O(3P) and O(1D).

Response: Thank you and I have revised it.

Line 60: "....the only significant chemical source...."

Response: Thank you and I have revised it.

Line 63-64: which is the only significant chemical source of ozone in the troposphere (Finlayson-Pitts et al., 2000).

Lines 68-71: Remove the symbol “S” in the brackets. It may be added as an index to “sigma” and “phi” but “S” is no variable like “lambda” or “T”.

Response: Thank you and I have revised it.

Lines 78-79: “Scattering aerosols can enhance..., while absorptive aerosols reduce ...throughout the boundary layer.” These statements are unclear and certainly do not apply for all conditions.

Response: I agree with you that these statements are unclear and certainly do not apply for all conditions. Therefore, I add “Some previous studies showed that” in front of this sentence. Both the abstract of Dickerson et al. (1997) and the introduction of Flynn et al. (2010) have put forward this viewpoint.

Reference:

Dickerson, R. R., Kondragunta, S., Stenchikov, G., Civerolo, K. L., Doddridge, B. G., Holben, N.: The impact of aerosols on solar ultraviolet radiation and photochemical smog, Science, 278, 827–830, 10.1126/science.278.5339.827, 1997.

Flynn, J., Lefer, B., Rappenglück, B., Leuchner, M., Perna, R., Dibb, J., Ziemba, L., Anderson, C., Stutz, J., Brune, W., Ren, X. R.: Impact of clouds and aerosols on ozone production in Southeast Texas. ATMOSPHERIC ENVIRONMENT, 44, 4126–4133, 10.1016/j.atmosenv.2009.09.005, 2010.

Line 85-88: Previous studies showed that scattering aerosols can enhance the actinic flux throughout the troposphere, while absorptive aerosols reduce the actinic flux throughout the boundary layer (Jacobson, 1998; Dickerson et al., 1997; Castro et al., 2001; Flynn et al., 2010).

Line 91: “Therefore it is necessary to quantitatively evaluate the effect of aerosols on photolysis frequencies for the purpose of ozone prevention”. I would say: “... for a better understanding of ozone formation under highly polluted conditions.”

Response: Thank you and I have revised it.

Line 98: Therefore, it is necessary to quantitatively evaluate the effect of aerosols on photolysis frequencies for a better understanding of ozone formation under highly polluted conditions.

Line 98: “... are compared with the observed value to test the simulation effect.” Unclear: If radiative transfer models are used there are usually no measurements available. And what is the “simulation effect”?

Response: The expressed meaning is unclear and thus I simplified this sentence.

Line 105: The observed data of related influential factors of the photolysis frequencies are taken as the model’s input to calculate the photolysis frequencies.

Line 100: “... due to complicated environmental conditions...“. Clarify.

Response: The complicated environmental conditions will influence the simulation of photolysis frequencies by radiative transfer model. Although AOD is easily acquired from ARONET and satellite, SSA, asymmetry factor, AE and the vertical profile of aerosols are not always available, and their observed values often had a large uncertainty. The complicated environmental conditions including relative humidity, temperature, planetary boundary layer height and emission characteristics all influence aerosol optical properties and thus influence light extinction of aerosols. Previous studies indicated that the aging of black carbon, mixing state of aerosols, the absorptive capacity of organic aerosols and the hygroscopicity of aerosols, all of which are determined by specific environmental condition, significantly contribute to the uncertainty of aerosol

optical properties and thus influence of the simulation of photolysis frequencies by radiative transfer model (Liao et al., 1999; Moffet et al., 2009; Gyawali et al., 2009; Lack and Cappa, 2010; Barnard et al., 2008; Jeong and Sokolik., 2007).

Reference:

Liao, H., Yung, Y. L., and Seinfeld, J. H.: Effects of aerosols on tropospheric photolysis rates in clear and cloudy atmospheres, JOURNAL OF GEOPHYSICAL RESEARCH, 104(D19), 23697–23707, 1999.

Moffet, R. C. and Prather, K.: In-situ measurements of the mixing state and optical properties of soot with implications for radiative forcing estimates, P. Natl. Acad. Sci., 106(29), 11872–11877, 2009.

Gyawali, M., Arnott, W. P., Lewis, K., and Moosmüller, H.: Insitu aerosol optics in Reno, NV, USA during and after the summer 2008 California wildfires and the influence of absorbing and non-absorbing organic coatings on spectral light absorption, Atmos. Chem. Phys., 9, 8007–8015, doi:10.5194/acp-9-8007-2009, 2009.

Lack, D. A. and Cappa, C. D.: Impact of brown and clear carbon on light absorption enhancement, single scatter albedo and absorption wavelength dependence of black carbon, Atmos. Chem. Phys., 10, 4207–4220, doi:10.5194/acp-10-4207-2010, 2010.

Barnard, J. C., Volkamer, R., and Kassianov, E. I.: Estimation of the mass absorption cross section of the organic carbon component of aerosols in the Mexico City Metropolitan Area, Atmos. Chem. Phys., 8, 6665–6679, doi:10.5194/acp-8-6665-2008, 2008.

Jeong, G. R; Sokolik, I. N., Effect of mineral dust aerosols on the photolysis rates in the clean and polluted marine environments. JOURNAL OF GEOPHYSICAL RESEARCH-ATMOSPHERES, 112, D21, 2007.

Line 123-136: Use the term “photolysis frequencies” consistently throughout the text.

Response: Thank you and I have revised it.

Lines 134, 135: Mind significant digits, see abstract by Li et al., 2011.

Response: Thank you and I have revised it.

Line 142-146: This study showed that the daily average j(O^1D) in the troposphere at the altitude of 1 km, 3 km, and 10 km from the ground was reduced by 53%, 37%, and 21%, respectively, resulting in a decrease in the ozone concentration by 5.4%, 3.8%, and 0.10% in the three layers.

Line 143ff: "Our overall goal..." It should be made clear that this study was strongly informed by a similar work by Gerasopoulos et al., 2012 which is not adequately referred to in the Introduction.

Response: Thank you and I have added this part.

Line 157-159: The relationship between AOD and photolysis frequencies is adequately compared with previous study in the Mediterranean (Casasanta et al., 2011; Gerasopoulos et al., 2012).

Line 155: The exact measurement period should be given here. Was it exactly four years?

Response: I have described the exact measurement period.

Line 161: From August 2012 to December 2015, j(O^1D) and j(NO_2) were measured continuously at PKUERS site. The data of the period during October 2012 to March 2013 and August 2015 are missed due to instrument maintenance and other measurement campaigns.

Line 163: What absorption cross sections and quantum yields were used to calculate the photolysis frequencies?

Response: The quantum yields of $J(O^1D)$ was taken from Matsumi et al.(2002), while the ozone cross section was derived from Daumont et al. (1992) and Malicet et al. (1995). For $j(NO_2)$, the quantum yields used was taken from Bass et al. (1976) and Davenport et al. (1978), while the cross section was derived from Jones and Bayes (1973), Harker et al. (1977) and Davenport (1978). I have added these sentences in the Manuscript.

Line 186-191: For $j(O^1D)$, the quantum yield used was taken from Matsumi et al.(2002), while the absorption cross section was derived from Daumont et al. (1992) and Malicet et al. (1995). Measured temperature was used to retrieve ozone absorption cross section and quantum yield. For $j(NO_2)$, the quantum yields used was taken from Bass et al. (1976) and Davenport et al. (1978), while the absorption cross section was derived from Jones and Bayes (1973), Harker et al. (1977) and Davenport (1978).

Line 163: I assume the j(O1D) were calculated temperature dependent according to Eq. 1 (and a statement in lines 302-304). That should be clearly stated. However, is it useful, if a common parameterization as a function of AOD is later used for summer and winter j(O1D)? There may be arguments to include temperature but the influence should be mentioned and quantified in Section 3 (see below).

Response: The j(O1D) were calculated temperature dependent. I added the sentence "Measured temperature are used to retrieve ozone absorption cross section and photodissociation quantum yield." in line 188. I have evaluated the impact of temperature on $j(O^1D)$ by calculating the ratio of $j(O^1D)$ to $j(O^1D)$ at temperature=298K (Figure S2). The result indicates that temperature changed $j(O^1D)$ by no more than 20%. In addition, the determination coefficients of fitted parametric equations are larger than 0.95, indicating the influence of temperature is relatively

small.

Line 458-469: For $j(O^1D)$, both of O_3 column and temperature affect $j(O^1D)$ significantly. Figure S1 presents the dependence of $j(O^1D)$ on ozone column at low AOD level (AOD<0.3) and SZA of (a) 30°±1° and (b) 60°±1°, respectively. Ozone column ranging from 270 to 400 DU leads to $j(O^1D)$ reducing about 50%. In order to evaluate the impact of temperature on $j(O^1D)$, we calculated the ratio of $j(O^1D)$ at measured temperature to $j(O^1D)$ at temperature = 298K ($j(O^1D)/ j(O^1D)_{T=298K}$) (Figure S2). $j(O^1D)/j(O^1D)_{T=298K}$ varied from 0.82 to 1.03 indicating that temperature changed $j(O^1D)$ by no more than 20%. Therefore, temperature played a minor role in changing $j(O^1D)$ compared with ozone column. As a result, when we fitted the relationship among $j(O^1D)$, AOD and cos(SZA), the effect of ozone column is considered but the effect of temperature is not considered.

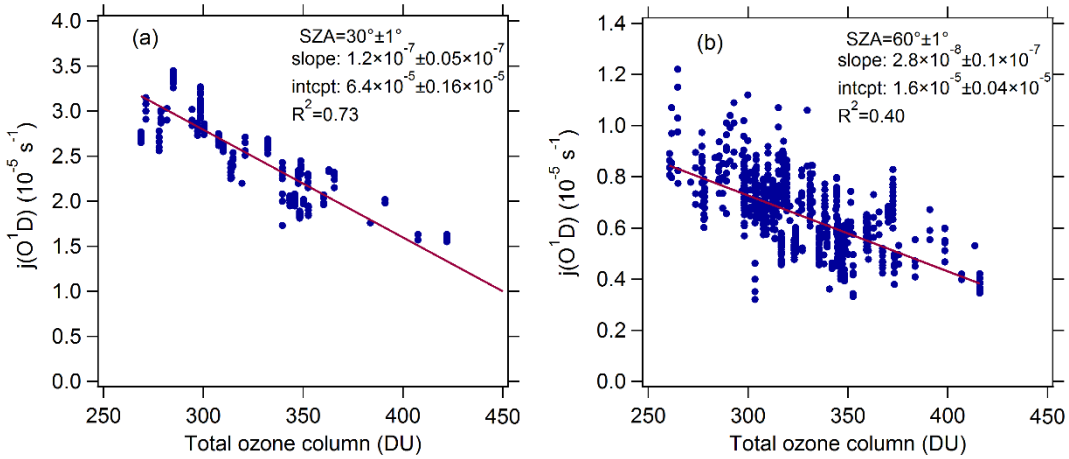

Figure S1. Dependence of $j(O^1D)$ on AOD (380nm) at low AOD level (AOD<0.3) and SZA of (a) 30°±1° and (b) 60°±1°, respectively.

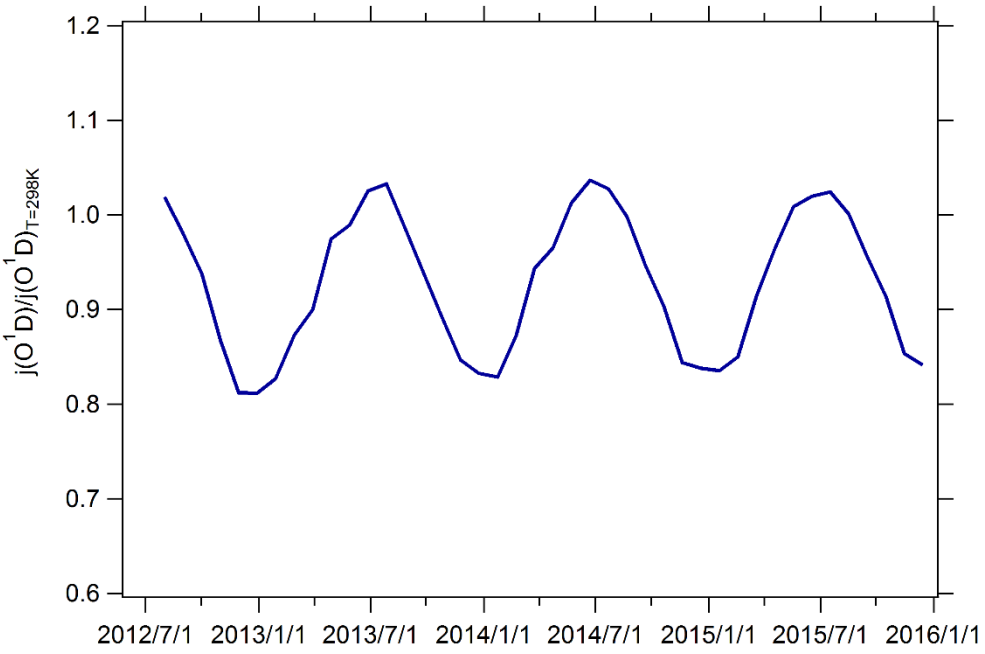

Figure S2. The time series of the monthly mean ratio of $j(O^1D)$ to $j(O^1D)_{T=298K}$ ($j(O^1D)/ j(O^1D)_{T=298K}$) from August 2012 to December 2015.

Line 164: "Shetter and Müller, 1999"

Response: Thank you and I have revised it.

Line 169: The studies by Shetter and Müller, 1999, and Hofzumahaus et al., 1999 describe double-monochromator based instruments with somewhat different properties.

The authors should state what type of detector was used and how regular calibrations of the instrument were performed during the four-year period. Moreover, it is unclear if the 10% uncertainty comes from the calibration uncertainty or is attributed to the uncertainties of absorption cross sections and quantum yields.

Response: (1) The double-monochromators for wavelength separation and successive measurements with single detectors (e.g. photomultipliers) upon scanning the wavelength. This is excellent for stray light suppression which is important in the

UV-B range (e.g. Shetter and Müller, 1999; Hofzumahaus et al., 1999). Drawbacks are the comparatively long time periods to complete the wavelength scans (≥30s) and the use of motor-driven optical components which may cause stability problems under field measurement conditions. Our method uses single monochromators and detector arrays (e.g. photodiode arrays) for simultaneous measurements covering the whole range of relevant wavelengths. This method has the advantage of high time-resolution and stability because no movable parts are involved. (2) The detector is a 2048×64 pixels photodiode array detector. (3) The 10% uncertainty is associated with the quartz receiver and stray-light effects.

Line177-194: The actinic flux was measured using a spectroradiometer and the photolysis frequencies were calculated from the absorption cross section and quantum yield of each species (Shetter and Müller, 1999). The spectroradiometer consisted of a single monochromator with a fixed grating (CARL ZEISS), an entrance optic with a 2π steradian (sr) solid angle quartz diffusor and a 2048×64-pixel photodiode array detector. The spectral measurements were performed with a wavelength resolution of 2 nm, covering a wavelength range of 290-650 nm (Hofzumahaus et al., 1999). A 1000 W National Institute of Standard and Technology (NIST) traceable lamp was used for calibration under laboratory conditions (Bohn et al., 2008). The measured spectra were corrected for dark signal and stray light. For $j(O^1D)$, the quantum yield was taken from Matsumi et al.(2002), while the ozone cross section was derived from Daumont et al. (1992) and Malicet et al. (1995). Measured temperature was used to retrieve ozone absorption cross section and quantum yield. For $j(NO_2)$, the quantum yield was taken from Bass et al. (1976) and Davenport et al. (1978), while the cross section was derived from Jones and Bayes (1973), Harker et al. (1977) and Davenport (1978). The calculated photolysis frequencies had a time resolution of 10 s and an accuracy of ±10% including uncertainties associated with the quartz receiver and stray-light effects.

Reference:

Matsumi, Y., Comes, F.J., Hancock, G., Hofzumahaus, A., Hynes, A.J., Kawasaki, M.,

Ravishankara, A.R., Quantum yields for production of $O(^1D)$ in the ultraviolet photolysis of ozone: recommendation based on evaluation of laboratory data. Journal of Geophysical Research 107 (D3), 4024. doi:10.1029/2001JD000510. 2002.

Daumont, D., Brion, J., Charbonnier, J., Malicet, J. Ozone UV spectroscopy I: absorption cross-sections at room temperature. Journal of Atmospheric Chemistry 15 (2), 145-155, 1992.

Malicet, J., Daumont, D., Charbonnier, J., Parisse, C., Chakir, A., Brion, J. Ozone UV spectroscopy. II. Absorption cross-sections and temperature dependence. Journal of Atmospheric Chemistry 21 (3), 263-273, 1995.

Bass, A. M., Ledford, A, E,, and Laufer, A. H., Extinction coefficients of NO_2 and N_2O_4, J. Res. Nat. Bureau Standards, 80A, 143-162, 1976.

Davenport, J.E. Determination of NO_2 photolysis parameters for stratospheric modelling, FAA Report No. FAA-EQ-7-14, 1978.

Jones, I. T. N. and Bayes, K. D., Photolysis of nitrogen dioxide, J. Chem. Phys. 59, 4836-4844, 1973.

Harker, A. B., Ho, W., and Ratto, J. J. Photodissoclation quantum yields of NO_2 in the region 375 to 420 nm, Chem Phys. Lett. 50, 394-397, 1977.

Line 175: "... close to the PKUERS site" should be specified in km.

Response: Thank you and I have specified the distance.

Line 195-198: The optical properties of aerosols were measured by a CIMEL solar photometer (AERONET level 2 data collection, http://aeronet.gsfc.nasa.gov/) and the site selected is the Beijing-CAMS site (39.93°N, 116.32°E), which is 6.4km from the PKUERS site.

Line 184: "This wavelength (380 nm) was chosen as it is more representative of j(NO2)"

Why wasn't the AOD at 340 nm used as well to estimate AODs more representative

for j(O1D) (around 300 nm), e.g. by the Angstrom equation? You can argue with better

comparability with Gerasopoulos et al. , 2012 but that should be made clear.

Response: Thank you and I have added the sentence "Additionally, at this wavelength we can better compare with the results of Gerasopoulos et al. (2012)."

Line 207-208: Additionally, at this wavelength we can better compare with the results of Gerasopoulos et al. (2012).

Line 185: SSA measurements during a period of one month are hardly representative for four years. Since the AOD-SSA relationship becomes important later to explain the steep decrease of j-values with AOD, I wonder why AERONET based SSA are not consulted for the whole period.

Response: In addition to our study, similar results in other regions have been obtained by Bais et al., 2005, Krotkov et al., 2005 and Kazadzis et al., 2012). We didn't use AERONET based SSA because that: (1) AERONET based SSA have a large uncertainty than that by ground based instruments; (2) There are only 10-20 data of SSA in a month for most months, which is much fewer than AOD data. The following figure is the relationship between AOD and AERONET based SSA during 2012-2015. There is a slight positive correlation between AOD and AERONET based SSA.

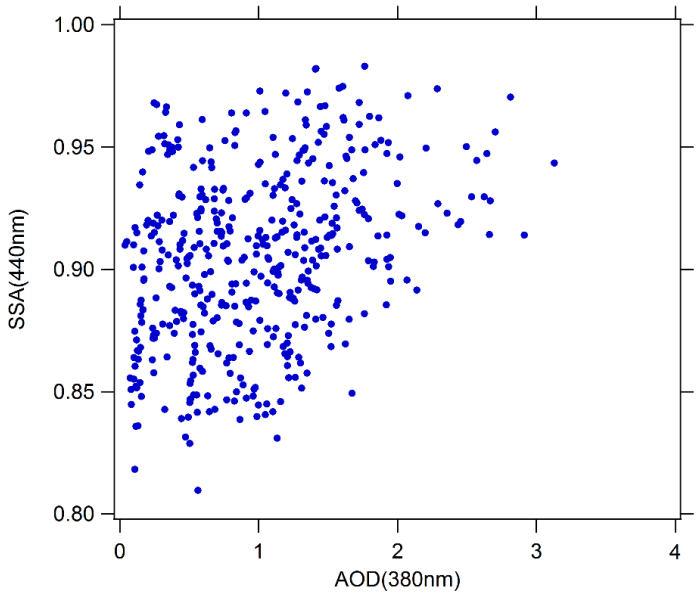

Figure 1. The relationship between AOD and AERONET based SSA.

Line 390-391: Similar results in other regions have been obtained by Bais et al., 2005, Krotkov et al., 2005 and Kazadzis et al., 2012).

Line 191: The source of the ozone column data should be specified and a citation included.

Response: Thank you and I have added the website of the ozone column data and related citation.

Line 215-217: The total ozone column was obtained by OMI (Ozone Monitoring Instrument) for the year 2012-2015, using overpass data (http://www.temis.nl/protocols/O3global.html) (Henk et al., 2003).

Line 198: "... under cloudless conditions." Was there an additional cloud screening performed or was any period marked cloud-free by AERONET taken? Because of the distance between the sites there were certainly some cases when clouds were present at PKUERS and no clouds at the AERONET site? Moreover, to assess the importance of this work, it would be interesting to learn what fractions of daytimes were identified

as clear-sky during the four years. This could be included in Table 2 for the different seasons.

Response: (1) The cloudless conditions are identified according to the presence of AOD data in AERONET since AOD data is unavailable under cloudy conditions. However, we didn't have additional cloud screening procedure. (2) I agree with you that the distance between the sites will cause some cases when clouds were present at PKUERS and no clouds at the AERONET site, which may disturb our analysis of the relationship between AOD and photolysis frequencies. Due to the close distance between the two sites (6.4km), this influence maybe relatively small. (3) Many thanks.

I added daytime clear-sky fraction for the different seasons in Table 2.

Line 208-210: The daytime clear-sky conditions were identified according to the presence of AOD data of AERONET since AOD data are unavailable under cloudy conditions.

Line 219-221: Table 1 presents O_3 column concentration, temperature, relative humidity, daytime clear-sky fraction and respective standard deviation for different seasons.

Line 1019:

Table 1. O_3 column concentration, temperature, relative humidity, daytime clear-sky fraction and respective standard deviation for different seasons.

Season	O_3 column (Du)	Temperature (℃)	Relative humidity (%)	Clear-sky fraction(%)
Spring	355±37	16±7.8	33±18	41
Summer	310±24	28±4.2	57±18	36
Autumn	304±23	16±7.4	46±21	42
Winter	347±28	0.53±4.2	30±18	41

Line 203: "Global irradiance" is a different quantity than actinic flux.

Response: Thank you and I have changed "Global irradiance" into "actinic flux spectra".

Line 231-234: In order to solve the radiative transfer equation, TUV uses the discrete-ordinates algorithm (DISORT) with 4 streams and calculates **the actinic flux spectra** with wavelength range of 280-420 nm in 1 nm steps and resolution.

Line 204: Explain "AE". Were the AE taken from AERONET, was a constant AE used, or was AE set to zero to simulate with a wavelength-independent AOD? This is important later for the model measurement comparisons in Fig. 5.

Response: AE (380/550nm) are taken from AERONET and the mean value of 1.3 during August 2012 - December 2015 is used in TUV model to simulate the wavelength dependency of AOD.

Line 210-211: AE were also acquired from ARONET.

Line 239-240: AE(380/550nm) is taken from AERONET and the mean value of 1.3 during June 2012 - December 2015 is used in TUV model.

Line 205: Were mean Earth-Sun distances used in the calculations or were time, date and location specified? If not, were the measured j-values scaled to a common mean Earth-Sun distance?

Response: Mean Earth-Sun distances was used in the calculations of TUV model and measured j-values were scaled to the mean Earth-Sun distance.

Line 377-381: The observed j(O^1D) was at ozone column of 330-360DU and were scaled to the temperature of 298K. AE(380/550nm) = 1.3, ozone column = 345 and Temperature = 298K were used in TUV model for all simulations. Mean Earth-Sun distance was used in the calculations of TUV model and measured j-values were scaled to the mean Earth-Sun distance.

Line 205: Were the same absorption cross sections and quantum yields used to calculate j(O1D) and j(NO2) from TUV-derived spectra? What temperatures were used?

Response: Measured temperatures were used to calculate the absorption cross sections and quantum yields of j(O^1D). The absorption cross sections and quantum yields of j(NO2) at 298K were used since they are influenced negligibly by temperature.

Line 230-234: Equations E2, E3 are not self-explaining. At least give a citation where these formulas are rationalized and explain "θ".

Response: Many thanks. I have gave a citation and explained "θ".

Line 258-261: Net ozone production is equal to the reaction rate between peroxy radicals (RO_2 and HO_2) and NO minus the loss rate of NO_2 and O_3 as shown in E2, E3, and E4 a**s derived by Mihelcic et al. (2003)**.

Line 269-270: where θ is the fraction of O^1D from ozone photolysis that reacts with water vapor.

Lines 239-278: "In order to evaluate the extinction capacity..." The motivation to look into the relationship between PM2.5 and AOD should be made clearer and the results shown in Fig. 1 and Fig. 2 should be reassessed. Obviously, PM2.5 is not a good proxy to estimate AOD. Moreover, the summer-winter differences in the slopes in Fig. 1 are probably explainable by the different heights of the boundary layers alone and there is no basis to speculate about seasonal differences of aerosol optical properties unless you consult AERONET data. My conclusion of Sect. 3.1 and the first paragraph

of Sect. 3.2 would be that PM2.5 is not suitable to estimate AOD (and consequently, PM2.5 data are not used in the remainder of the text). On the other hand, did you check the relationship between PM2.5 and e.g. j(NO2) directly? I assume it looks much poorer than the relationship between j(NO2) and AOD which would confirm the assumption that AOD is a more relevant parameter.

Response: (1) I have revised the motivation to look into the relationship between PM2.5 and AOD. Compared with AOD, $PM_{2.5}$ is a more common proxy to evaluate the level of particulate matter pollution in spite that AOD is a more closely related parameter of photolysis frequencies. As a result, we attempted to analyze the quantitative relationship between $PM_{2.5}$ and AOD to evaluate the influence of $PM_{2.5}$ on AOD and thus on photolysis frequencies. (2) I agree with you that $PM_{2.5}$ is not a good proxy to estimate AOD due to multiple interference factors including relative humidity, planetary boundary layer height, aerosol type, aerosol size distribution, aerosol distribution in the vertical direction. Zheng et al. (2017) studied the influential

factors for the relationship between PM2.5 and AOD in Beijing during 2011-2015. He found that in addition to RH and PBLH, aerosol components (scattering or absorptive) and size (coarse mode or fine mode) also influenced the slope of PM2.5 vs AOD significantly according to SSA, AE and FMF data of AERONET. Since Zheng et al. (2017) have studied this question in detail in the same region and the same period, I think that our work needn't analyze SSA, AE and FMF data of AERONET again. Instead, we just compared the slope of PM2.5 vs AOD of our study with other study in Beijing and other cities of North China. I agree with you that the conclusion is that PM2.5 is not suitable to estimate AOD due to the large uncertainty. (3) I have checked the relationship between PM2.5 and j(NO2) directly, it is true that there is much poorer correlation than the relationship between j(NO2) and AOD.

Line 276-281: Compared with AOD, $PM_{2.5}$ is a more common proxy to evaluate the level of particulate matter pollution in spite that AOD is a more closely related parameter of photolysis frequencies. As a result, we attempted to analyze the quantitative relationship between $PM_{2.5}$ and AOD to evaluate the influence of $PM_{2.5}$ on AOD and thus on photolysis frequencies.

Line 307-308: Consequently, using $PM_{2.5}$ to estimate AOD has a large uncertainty due to multiple interference factors.

Line 249, Table 2: Table 2 should be mentioned in Section 2.1, not here. Please consider significant digits in Tab. 2 and specify season periods in the caption.

Response: Many thanks, and I have revised it. I change Table 2 into Table 1.

Line 218-222: In addition, meteorological parameters such as temperature, relative humidity, and pressure were simultaneously observed at this site. Table 1 presents total O_3 column, temperature, relative humidity, daytime clear-sky fraction and respective standard deviation for different seasons.

Line 1001-1004:

Table 1. O_3 column concentration, temperature, relative humidity, daytime clear-sky fraction and respective standard deviation for different seasons (spring: March, April and May; summer: June, July and August; autumn: September, October and November; winter: December, January and February).

Season	O_3 column (Du)	Temperature (℃)	Relative humidity (%)	Clear-sky fraction(%)
Spring	355±37	16±7.8	33±18	41
Summer	310±24	28±4.2	57±18	36
Autumn	304±23	16±7.4	46±21	42
Winter	347±28	0.53±4.2	30±18	41

Figs. 2-3: Specify what is shown here. Averages, medians? The periods defined as "spring", "summer", "autumn" and "winter" should be defined clearly somewhere. Are
the PM2.5 data in Fig. 2b also from clear-sky days only? Specify "AOD (380 nm)" in the caption of Fig. 2.

Response: (1) Figs. 2-3 show mean values. I have specified it. (2) Thank you, I have define "spring", "summer", "autumn" and "winter" in Line 285-287. (3) The previous PM2.5 data in figure 2b are from all-sky days. I have revised Figure 2b using PM2.5 data from clear-sky days.

Line 1133: Figure 2. Diurnal cycles of (a) mean AOD and (b) mean $PM_{2.5}$ in the four seasons under cloudless conditions.

Line 1152: Figure 3. Diurnal cycles of (a) mean $j(O^1D)$ and (b) mean $j(NO_2)$ in the four seasons under cloudless conditions.

Line 284-287: The determination coefficient (r^2) is 0.53, 0.58, 0.62 and 0.59 for spring (March, April and May), summer (June, July and August), autumn (September, October and November) and winter (December, January and February), respectively.

Lines 285-292: 1) What do the stated differences in photolysis frequencies refer to? Mean daily maxima? Please specify. 2) What are the uncertainties of these differences? 3) Does the TUV-derived difference refer to aerosol-free conditions? 4) What role plays the temperature, certainly lower in Beijing during the winter compared to conditions in Crete?

Response: 1) The stated differences in photolysis frequencies refer to mean daily maxima and I have specified it in the manuscript. 2) I have added the uncertainties of these differences. 3) Yes, the TUV-derived difference refers to aerosol-free conditions and I have specified it in the manuscript. 4) I have added the analysis of the influence of temperature during winter.

Line 326-330: The observed mean daily maxima of photolysis frequencies at this site are lower than that observed in the eastern Mediterranean (Crete, Greece, 35°20′N,25° 40′E) (Gerasopoulos et al., 2012) by $7.8\times10^{-6} \pm 5.5\times10^{-6}$ s^{-1} and $4.9\times10^{-6} \pm 1.8\times 10^{-6}$ s^{-1} for $j(O^1D)$, and $1.9\times10^{-3} \pm 1.2\times10^{-3}$ s^{-1} and $3.3\times10^{-3} \pm 1.0\times10^{-3}$ s^{-1} for $j(NO_2)$, in summer and winter respectively.

Line 330-334: The corresponding lower photolysis frequencies of Beijing than the eastern Mediterranean due to SZA difference is 1.7×10^{-6} s^{-1} and 3.0×10^{-6} s^{-1} for $j(O^1D)$, and 8.0×10^{-5} s^{-1} and 6.6×10^{-4} s^{-1} for $j(NO_2)$ according to TUV model under aerosol-free conditions, which are significantly lower than observed decreased magnitudes.

Line 334-339: Additionally, we know that the temperature is lower in Beijing during the winter compared to conditions in Crete. The measured mean temperature in Beijing during winter is equal to 0.53±4.2 °C (Table 1). When we consider the mean

temperature in Crete (about 10 °C) is 10 °C higher than in Beijing, the lower $j(O^1D)$ of Beijing than Crete is 5.5×10^{-7} s^{-1}, which is also not able to compensate the $j(O^1D)$ gap between the two regions during winter.

Fig. 4: Specify in the caption what the full lines show. Averages, medians? What AOD bin size was used? Indicate AOD (380 nm).

Response: The full lines are fitted by exponential function. The coefficients of determination (r^2) vary from 0.5 to 0.8. I have specified it in fig. 4.

Line 1168-1170: Figure 4. Dependence of $j(O^1D)$ on AOD (380nm) at SZA of (a) 30° and (b) 60° and at different classes of ozone column concentration: 300-330 DU (red), 330-360 DU (blue), and 360-390 DU (green). The full lines are fitted by exponential function.

Fig. 5: Add standard deviations to the measured values. Otherwise the relevance of the differences compared to the model calculations cannot be assessed. Specify the ozone column range of the measured data in the caption. Indicate AOD (380 nm) for the measured data and AOD ≠ f(λ) for the model calculations (if that applies).

Response: (1) I have add standard deviations to the measured values. (2) The ozone column range for $j(O^1D)$ is 330-360 DU. I have specified it.

Line 319-326: Here the question again arises, what AE was used in the TUV calculations, what temperatures and if the annual changes in Sun-Earth distances were considered.

Response: We used the mean AE=1.3, temperature = 298K in TUV. In addition, we used the mean Sun-Earth distance in TUV.

Line 377-381: The observed j(O^1D) is at temperature of 288-308K and ozone column of 330-360DU. AE(380/550nm) = 1.3, ozone column = 345 and Temperature = 298K are used in TUV model for all simulations. Mean Earth-Sun distance was used in the calculations of TUV model and measured j-values were scaled to the mean Earth-Sun distance.

Lines 327-341 and lines 341-347: These sections are too speculative without consulting AERONET data. As already mentioned, the 1-month data in Fig. 6 is probably not

representative for the average aerosol over the four year measurement period.

Response: As mentioned above, there is a slight positive correlation between AOD and AERONET based SSA during 2012-2015. As the AERONET based SSA data have a large uncertainty, we are not sure if the result should be added into the manuscript.

Lines 357-361 and Table 3: Consider significant digits.

Response: I have revised it.

Figure 7: What do the full lines show?

Response: The full lines are fitted by exponential function.

Line 1221-1223: Figure 7. Dependence of j(NO_2) on AOD (380nm) at different SZA classes. The classes of cos(SZA) are 0–0.2 (black), 0.2–0.4 (purple), 0.4–0.6 (green), 0.6–0.8 (blue), and 0.8–1 (red). The full lines are fitted by exponential function.

Line 397: Equation E5 should appear here.

Response: Thank you and I have revised it.

Lines 397-406, Tables 5 and 6: 1) If ozone columns have no significant influence on j(NO2), why does Tab. 5 give four different parametrizations for four different ozone column ranges? A single parametrization should be given here to make things easier for readers who want to use these formulas. 2) What is the nature of the error limits of the parameters a1-a6 and are they of any relevance to estimate the quality of the parameterizations? Please note that for j(NO2) most parameters vary more strongly if different ozone column ranges are compared than indicated by the errors of the param-

eters. So these errors have no relevance and pretend an accuracy that is not real. 3) Did you systematically test if simpler parameterizations give satisfactory results as well

by taking out single parameters? 4) For j(O1D) the parametrization appears arbitrary: parameters show no clear trend with ozone column although this would be expected even for an empirical formula. It would be more convincing to use a parameterization that contains SZA, AOD and ozone columns in a single formula. 5) Given that the data

were probably (i) not normalized to a common Sun-Earth distance, nor (ii) to the same

temperature; (iii) the AOD (380 nm) used does not apply strictly to the j(O1D) wave-length range, (iv) only 30 DU wide ranges of ozone columns were merged, and (v) cloud-sceening cannot be perfect, the obtained r2>0.95 is remarkable, also compared to Tab. 3 and 4, and should be rationalized.

Response: 1) I agree with you that a single parametrization should be given for j(NO_2). I have revised it. 2) The error limits refer to 95% confidence bounds of these parameters. When we used a single parametric equation for all data of j(NO_2), the error limits get lower significantly than that of different ozone column classes. 3) Yes,

I try using different functions to fit the relationship, and it seems that the quadratic polynomial form gave the best fit, which reflects the nonlinear relationship between AOD and j-values and considers the combined effect of the AOD and SZA on j-values.

4) I agree with you that it would be more convincing to use a parameterization that contains SZA, AOD and ozone columns in a single formula. I have revised it in this part. 5) All of the problems of the data you have mentioned is true. Even if there are these problems in the data, I acquired a remarkable r2 (r2>0.95), indicating the fitted results is relatively rationalized.

Line471:

$$j(NO_2) = a_1 + a_2 AOD + a_3 cos(SZA) + a_4 (AOD)^2 + a_5 AOD cos(SZA) + a_6 (cos(SZA))^2$$

.....E5

Line 464-470: By fitting the relationship at different ozone classes (classification width=30DU), we found that ozone column increasing by 30DU results in $j(O^1D)$ at a constant SZA and AOD decreasing by 18%. Therefore, the parametric equation for $j(O^1D)$ is transformed into the form E6, which reflects the influence of ozone column. The parameters a_1-a_6 correspond to ozone column range = 300-330 DU, thus we use 315 DU as the weighted standard of ozone column. The fitting parameters a_1-a_6 for $j(O^1D)$ is shown in Table 6.

$$j(O^1D) = [a_1 + a_2 AOD + a_3 cos(SZA) + a_4 (AOD)^2 + a_5 AOD cos(SZA) + a_6 (cos(SZA))^2] \times [1+(315 - O_3 \text{ column}) \times 0.006]$$

……E6

Lines 407-409: What do the percentage reductions refer to? See also abstract and conclusions.

Response: The percentage reductions refer to seasonal mean values under clear-sky conditions. I have revised it.

Line 485-490: The parametric equations can be used to quantitatively evaluate the effect of AOD on photolysis frequencies in Beijing. According to the parametric equations, aerosols lead to a decrease in seasonal mean $j(NO_2)$ by 24% and 30% and a

decrease in seasonal mean j(O^1D) by 27% and 33% in summer and winter under clear-sky conditions, respectively, compared to an aerosol-free atmosphere.

Line 411: "... and lower SSA in winter" Was not shown.

Response: I have removed "... and lower SSA in winter".

Lines 431-433: As mentioned above, this statement is not justified and the use of PM2.5 would most likely lead to no improvement of estimated j(O1D) or j(NO2) unless you can show it directly.

Response: Yes, the use of PM2.5 leads to no improvement of estimated j(O1D) or j(NO2). Therefore, I have removed this part.

Line 460, Figure 8: I assume what is shown in Fig. 8, and the 25% reduction stated in the text, refer to mean daytime ozone productions. Please specify time period.

Response: Yes, it refer to mean daytime ozone productions and I have revised it.

Line 541-543: Figure 8. Since the decreasing amplitude of the daytime ozone production rate is far larger than that of the daytime ozone loss rate, the mean daytime net production rate of ozone is reduced by 25%.

Line 1237: Figure 8. Mean daytime ozone production and loss terms in August 2012.

Figure 9: How were the data shown derived, i.e. what periods of time do single data points represent?

Response: Single data point represent daytime hourly mean value.

Line 1250-1251: Figure 9. Correlation between $P(O_3)_{j\_obs}/P(O_3)_{j\_AOD=0}$ (or $D(O_3)_{j\_obs}/D(O_3)_{j\_AOD=0}$) and JIF of $j(NO_2)$. Single data point represent daytime hourly mean value.

Figure 10: Indicate in the caption that the data represent mean values over a period of one month (or n clear-sky days) in August 2012.

Response: I have specified it in the caption.

Line 1267-1268: Figure 10. Diurnal profiles of mean $P(O_3)_{j\_obs}$, $P(O_3)_{j\_AOD=0}$, $D(O_3)_{j\_obs}$, and $D(O_3)_{j\_AOD=0}$ in August 2012 under clear-sky conditions.

Figure 11: In the caption refer to Table 7 to explain the meaning of day A and day B.

Response: I have specified it in the caption.

Line 1281-1286: Figure 11. Diurnal profile of net $P(O_3)$ simulated by the box model. Three cases are displayed: (1) A day (red circles): August 21, 2012 with low AOD level and high photolysis frequencies; (2) B day (blue circles): August 26, 2012 with high AOD level and low photolysis frequencies; and (3) the photolysis frequencies of B day adjusted to the level of A day with other conditions unchanged (green circles). The specific conditions of A day and B day are listed in Table 7.

Table 7, 8: Mind significant digits.

Response: I have revised it.

Anonymous Referee #2

1) In the introduction, after the definition of actinic flux (line 68) the authors could include that since the photolysis rates are proportional to the actinic flux and not all stations acquire a 2π spectroradiometer or chemical actinometers for J measurements, several methods have been developed to determine actinic flux and photolysis rates from ground based measurements of irradiance (Kylling et al 2003, Kazadzis et al. 2000,

2004, Topaloglou et al. 2005, Trebs et al. 2009).

Response: Thank you and I have added this sentence in the manuscript.

Line 69-74: Since the photolysis rates are proportional to the actinic flux and not all stations acquire a 2π spectroradiometer or chemical actinometers for J measurements, several methods have been developed to determine actinic flux and photolysis frequencies from ground based measurements of irradiance (Kylling et al 2003, Kazadzis et al. 2000, 2004, Topaloglou et al. 2005, Trebs et al. 2009).

---

2) It is stated, in the abstract, that the reduction of J(O1D) and J(NO2) is in the order of 24.2% and 30.4% (for summer and winter respectively) while for the J(NO2) in the order of (27.3 an 32.6%) compared to an aerosol free atmosphere (aod=0?). Since the parametric equations include sza and AOD, the authors could clarifiy how exactly these

percentages have been calculated i) to what sza are these percentages referring to? Also for what ozone class for J(O1D)? ii) are these maximum reductions for maximum

aod observed or for a mean aod value (i.e. 0.76)? iii) Through which parameters are summer and winter percentages calculated?

Response: Aerosol free atmosphere refers to AOD=0, and I specified it in the manuscript. We use the parametric equations (Table 5 and Table 6) to calculated

J(O1D) and J(NO2) using corresponding SZA and AOD at corresponding time (5 minute average). Two situations are calculated: One, AOD is equal to 0 at all times. Two, AOD is equal to the observed values at all times. For the calculation in the two situations, the corresponding parametric equation at different ozone classes is used according to observed ozone column at different times. The mean values of J(O1D) and J(NO2) for summer and winter are calculated in the two situations and the reduction ratio can be calculated accordingly.

---

3) How do the authors comment the (low) r2 coefficient in the linear fits of J(O1D) and J(NO2) versus aod for aod<0.7?

Response: For j(NO2), the relatively large SZ classification width (0.2) is the main cause of the low r2. If we shrink SZ classification width into 0.05, the r2 coefficient will be higher than 0.6. For j(O1D), the relatively large ozone column classification width (30DU) contributes to the low r2 to a large extent. In addition, the nonlinear relationship between j-values and AOD also leads to the low r2 for AOD<0.7.

---

4) Concerning the TUV radiation model, information (apart from ssa values) about the input that was used could be included, such as solar spectrum used, aerosol profile etc.

In p.2.2 it is stated that global irradiance spectra are calculated. Do you maybe mean actinic flux spectra? Since photolysis rates are proportional to actinic flux, has any comparison been done between the actinic flux measured by the spectroradiometer and that from the TUV model in order to demonstrate the level of agreement?

Response: (1) TUV uses the discrete-ordinates algorithm (DISORT) with 4 streams and calculate the actinic flux spectra with wavelength range of 280-420 nm in 1 nm steps and resolution. I have added it in the manuscript. Aerosol profile is given by Elterman (1968). (2) I have changed global irradiance spectra into actinic flux spectra.

(3) I have simulated actinic flux by TUV to compare with observed results during August 2012, when we have observed SSA data. The agreement between simulation and observation is within 15%. For other time, the simulation couldn't be carried out well due to lack of measured SSA data.

Line 206-210: In order to solve the radiative transfer equation, TUV uses the discrete-ordinates algorithm (DISORT) with 4 streams and calculates actinic flux spectra with wavelength range of 280-420 nm in 1 nm steps and resolution. Measured temperatures were used to calculate the absorption cross sections and quantum yields.

---

5) In line 419, the enhanced aerosol level in Bejing is quantified (4-year mean aod = 0.76±0.76). Some references to the studies should be included.

Response: The 4-year mean AOD=0.76±0.75 is calculated by observed AOD during 2012-2015.

---

6) In Line 254: "....according to another study in urban Bejing, ..", the reference of the study should be included.

Response: Thank you and I have added the reference.

Line 262-264: According to another study in urban Beijing, the higher the RH, the smaller the slope, and the higher the PBLH, the smaller the slope (Zheng, C. W et al., 2017).

---

7) Figure 6: Similar results have been obtained by Bais et al., 2005, Krotkov et al., 2004

and Kazadzis et al., 2017). Is this AOD -SSA dependence from August 2012 obvious during all seasons ? For which wavelength are SSA values given? As both parameters have a wavelength dependence and since PF ozone "effective" wavelengths are ~305-315nm, could this dependence play some role in the provided analysis of the AOD

and

SSA effects on PFs. ?

Response: Thank you, I have added the sentence "Similar results have been obtained by Bais et al., 2005, Krotkov et al., 2005 and Kazadzis et al., 2017)." In the manuscript. We just observed SSA in August 2012 and thus the AOD-SSA dependence is just available in summertime but unavailable in other seasons. SSA values are at 525nm. The following figure is the relationship between AOD and AERONET based SSA (440nm) during 2012-2015 for all seasons. There is a slight positive correlation between AOD and SSA during 2012-2015 for all seasons. We didn't use AERONET based SSA in this study because that: (1) AERONET based SSA have a large uncertainty; (2) There are only 10-20 data of SSA for most months, which is much fewer than AOD data. Sorry, I don't understanding the meaning of PFs.

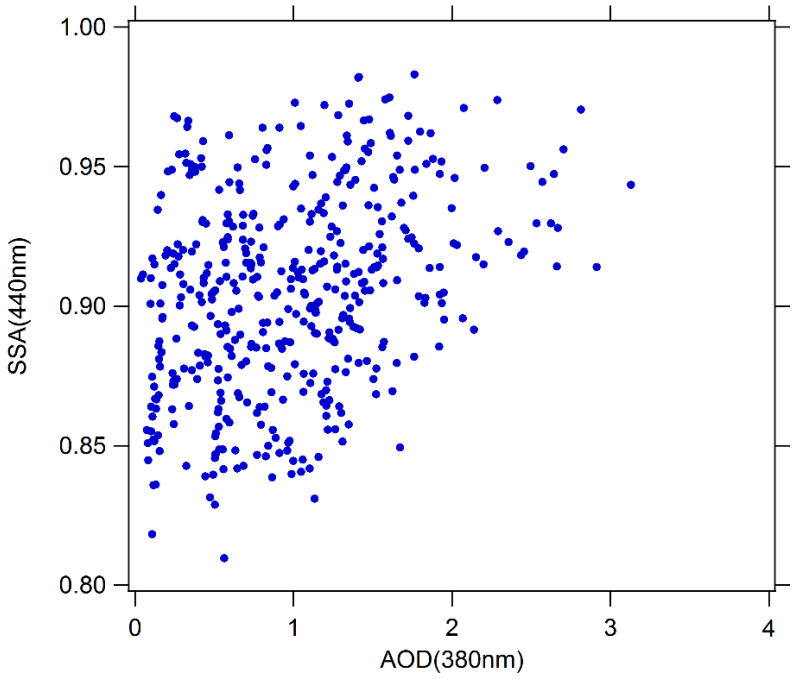

Figure 1. The relationship between AOD and AERONET based SSA.

Line 343-344: Similar results have been obtained by Bais et al., 2005, Krotkov et al., 2005 and Kazadzis et al., 2012.

---

8) Figures 4 and 7: Some commentation on the scatter of J's would be helpful Technical corrections.

Response: Thank you and I have added some comments on the scatter of J versus AOD in page 16 and page 19.

Line 324-325: The scatter of these points is mainly due to variations in ozone column and temperature.

Line 388-389: The scatter of these points is due to the relatively large classification width of SZA to a large extent.

Line 249-250: Repetition of "in summer" "This implies that the aerosols in summer have stronger extinction capacity in summer than in winter"

Response: Thank you and I have revised it.

Line 257-258: This implies that the aerosols in summer have stronger extinction capacity than in winter.

Lines 384 &385: cos(SZA) instead of SZA

Response: Thank you and I have revised it.

Line 398-402: The slope of j(NO_2) vs AOD also displays a significant dependence on cos(SZA). The slope increases as cos(SZA) increases from 0 to 0.5 and then decreases as cos(SZA) increases from 0.5 to 1.

Line 423: "..The result of this study is comparable to the reduction ratio of this study possibly due to..". Probably the one "this study" refers to the previous study mentioned,

Hodzie et el. 2007 and the second one to the authors study, it would be helpful to rephrase.

Response: Thank you and I have revised it. "..The result of Hodzic et al. (2007) is comparable to the reduction ratio of this study possibly due to.."

Line 437-438: The result of Hodzic et al. (2007) is comparable with the reduction

ratio of this study possibly due to the equivalent levels of AOD and SSA.

Line 559: "...in August 2014..", refers to the field campaign in August 2012, mentioned

in the paper.

Response: Thank you and I have revised it.

Line 572-573: In order to evaluate the effects of aerosols on ozone production rate, we carried out an observation campaign in August 2012.

A list of all relevant changes made in the manuscript:

The relevant manuscript changes are noted in red text.

Line 27: Both $j(O^1D)$ and $j(NO_2)$ display significant dependence on AOD (380nm) with a nonlinear negative correlation.

Line 30-34: the actinic flux decreases with AOD. The absolute values of slopes are equal to 4.2-6.9▪10^{-6} s^{-1} and 3.2▪10^{-3} s^{-1} per AOD unit for $j(O^1D)$ and $j(NO_2)$ respectively at SZA of 60° and AOD smaller than 0.7, both of which are larger than those observed in a similar, previous study in the Mediterranean.

Line 34-36: This indicates that the aerosols in urban Beijing have a stronger extinction effect on actinic flux than absorptive dust aerosols in the Mediterranean.

Line 39-42: According to the parametric equation, aerosols lead to a decrease in seasonal mean $j(NO_2)$ by 24% and 30% for summer and winter, respectively, and the corresponding decrease in seasonal mean $j(O^1D)$ by 27% and 33% respectively, compared to an aerosol-free atmosphere (AOD = 0).

Line 44-46: The simulation results shows that the monthly mean daytime net ozone production rate is reduced by up to 25% due to the light extinction of aerosols.

Line 61-64: In addition, the photolysis of NO_2 produces O^3P, and then O^3P reacts with O_2 to produce O_3, as shown by reactions R3 and R4, which is the only significant chemical source of ozone in the troposphere (Finlayson-Pitts et al., 2000).

Line 72-77: Since the photolysis rates are proportional to the actinic flux and not all stations acquire a 2π spectroradiometer or chemical actinometers for J measurements, several methods have been developed to determine actinic flux and photolysis frequencies from ground based measurements of irradiance (Kylling et al 2003, Kazadzis et al. 2000, 2004, Topaloglou et al. 2005, Trebs et al. 2009).

Line 85-88: Previous studies showed that scattering aerosols can enhance the actinic flux throughout the troposphere, while absorptive aerosols reduce the actinic flux throughout the boundary layer (Jacobson, 1998; Dickerson et al., 1997; Castro et al., 2001; Flynn et al., 2010).

Line 98-100: Therefore, it is necessary to quantitatively evaluate the effect of aerosols on photolysis frequencies for a better understanding of ozone formation under highly polluted conditions.

The observed data of related influential factors of the photolysis frequencies are taken as the model's input to calculate the photolysis frequencies.

Line 107: This method

Line 132-133: Previous model studies have shown that aerosols in China can affect ozone production by changing the photolysis frequencies.

Line 136: photolysis frequencies

Line 146-147: Lou et al (2014) found that with aerosols, annual mean photolysis frequencies.

Line 157-158: The relationship between photolysis frequencies and AOD is adequately compared with previous study in the Mediterranean (Casasanta et al., 2011; Gerasopoulos et al., 2012).

Line 168-171: From August 2012 to December 2015, $j(O^1D)$ and $j(NO_2)$ were measured continuously at PKUERS site. The data of the period during October 2012 to March 2013 and August 2015 are missed due to instrument maintenance and other measurement campaigns.

Line 179: (Shetter and Müller, 1999)

Line 179-182: The spectroradiometer consisted of a single monochromator with a fixed grating (CARL ZEISS), an entrance optic with a 2π steradian (sr) solid angle quartz diffusor and a 2048×64-pixel photodiode array detector.

Line 183-185: A 1000 W National Institute of Standard and Technology (NIST) traceable lamp was used for calibration under laboratory conditions (Bohn et al., 2008).

Line 186-192: For $j(O^1D)$, the quantum yields used were taken from Matsumi et al.(2002), while the ozone cross section was derived from Daumont et al. (1992) and Malicet et al. (1995). Measured temperatures were used to retrieve ozone absorption cross section and quantum yield. For $j(NO_2)$, the quantum yields used were taken

from Bass et al. (1976) and Davenport et al. (1978), while the cross section was derived from Jones and Bayes (1973), Harker et al. (1977) and Davenport (1978).

Line 192-194: The calculated photolysis frequencies had a time resolution of 10 s and an accuracy of ±10% including uncertainties associated with the quartz receiver and stray-light effects (Edwards and Monks, 2003).

Line 195-198: The optical properties of aerosols were measured by a CIMEL solar photometer (AERONET level 2 data collection, http://aeronet.gsfc.nasa.gov/) and the site selected is the Beijing-CAMS site (39.93°N, 116.32°E), which is 6.4km from the PKUERS site.

Line 207-211: Additionally, at this wavelength we can better compare with the results of Gerasopoulos et al. (2012). The daytime clear-sky conditions were identified according to the presence of AOD data of AERONET since AOD data are unavailable under cloudy conditions. AE were also acquired from ARONET.

Line 211-212: The SSA (525nm) data were derived from a field campaign undertaken in August 2012.

Line 214-216: Five-minute averages of AOD, SSA, and photolysis frequencies were analyzed in this study.

Line 216-222: The total ozone column was obtained by OMI (Ozone Monitoring Instrument) for the year 2012-2015, using overpass data (http://www.temis.nl/protocols/O3global.html) (Henk et al., 2003). In addition, meteorological parameters such as temperature, relative humidity, and pressure were simultaneously observed at this site. Table 1 presents total O_3 column, temperature, relative humidity, daytime clear-sky fraction and respective standard deviation for different seasons.

Line 224-226: The relevant contents and methods of observation are shown in Table 2.

Line 231-233: We use the Tropospheric Ultraviolet and Visible (TUV) radiation model (version 5.3) provided by Sasha Madronich (Madronich, 1993).

Line 231-233: In order to solve the radiative transfer equation, TUV uses the

discrete-ordinates algorithm (DISORT) with 4 streams and calculates the actinic flux spectra with wavelength range of 280-420 nm in 1 nm steps and resolution. Measured temperatures and ozone column were used to calculate the absorption cross sections and quantum yields.

Line 237-240: The key aerosol optical properties including AOD, SSA and AE were input into the model to test the effect of aerosols on photolysis frequencies. AE(380/550nm) is taken from AERONET and the mean value of 1.3 during June 2012 - December 2015 is used in TUV model.

Line 261-263: Net ozone production is equal to the reaction rate between peroxy radicals (RO_2 and HO_2) and NO minus the loss rate of NO_2 and O_3 as shown in E2, E3, and E4 as derived by Mihelcic et al. (2003).

Line 272-273: where θ is the fraction of O^1D from ozone photolysis that reacts with water vapor. i and j represent the number of species of RO_2 and alkenes, respectively.

Line 278-284: Compared with AOD, $PM_{2.5}$ is a more common proxy to evaluate the level of particulate matter pollution in spite that AOD is a more closely related parameter of photolysis frequencies. As a result, we attempted to analyze the quantitative relationship between $PM_{2.5}$ and AOD to evaluate the influence of $PM_{2.5}$ on AOD and thus on photolysis frequencies.

Line 297-299: According to another study in urban Beijing, the higher the RH, the smaller the slope, and the higher the PBLH, the smaller the slope (Zheng, C. W et al., 2017).

Line 307-311: Compared with other cities in North China (Tianjin, Shijiazhuang and Baoding) (Ma et al., 2016), the slope in Beijing for winter is significantly higher. Consequently, using $PM_{2.5}$ to estimate AOD has a large uncertainty due to multiple interference factors.

Line 315-320: The diurnal cycles of AOD are shown in Figure 2. AOD displays obvious diurnal variation, with relatively high level at noon and low level at dawn and evening. The diurnal variation of $PM_{2.5}$ is - significantly different from AOD.

Line 329: The observed mean daily maxima of photolysis frequencies.

Line 336: under aerosol-free conditions.

Line 337-342: Additionally, we know that the temperature is lower in Beijing during the winter compared to conditions in Crete. The measured mean temperature in Beijing during winter is equal to 0.53±4.2 ℃ (Table 1). When we consider the temperature in Crete is 10 ℃ higher than in Beijing, the lower $j(O^1D)$ of Beijing than Crete is 5.5×10^{-7} s^{-1}, which is also not able to compensate the $j(O^1D)$ gap between the two sites during winter.

Line 364-366: This relatively large classification width is chosen to make sure that there are enough points to fit the relationship between $j(O^1D)$ and AOD.

Line 367-368: The scatter of these points is mainly due to variations in ozone column and temperature.

Line 377-382: The observed $j(O^1D)$ was at ozone column of 330-360DU and were scaled to the temperature of 298K. AE(380/550nm) = 1.3, ozone column = 345 and Temperature = 298K were used in TUV model for all simulations. Mean Earth-Sun distance was used in the calculations of TUV model and measured j-values were scaled to the mean Earth-Sun distance.

Line 390-391: Similar results in other regions have been obtained by Bais et al., 2005, Krotkov et al., 2005 and Kazadzis et al., 2012).

Line 436-437: The scatter of these points is due to the relatively large classification width of SZA to a large extent.

Line 459-476: The fitting parametric equations for $j(NO_2)$ is shown in Table 5. For $j(O^1D)$, both of O_3 column and temperature affect $j(O^1D)$ significantly. Figure S1 presents the dependence of $j(O^1D)$ on ozone column at low AOD level (AOD<0.3) and SZA of (a) 30°±1° and (b) 60°±1°, respectively. Ozone column ranging from 270 to 400 DU leads to $j(O^1D)$ reducing about 50%. In order to evaluate the impact of temperature on $j(O^1D)$, we calculated the ratio of $j(O^1D)$ at measured temperature to $j(O^1D)$ at temperature = 298K ($j(O^1D)/ j(O^1D)_{T=298K}$) (Figure S2). $j(O^1D)/j(O^1D)_{T=298K}$

varied from 0.82 to 1.03 indicating that temperature changed $j(O^1D)$ by no more than 21%. Therefore, temperature played a minor role in changing $j(O^1D)$ compared with ozone column. As a result, when we fitted the relationship among $j(O^1D)$, AOD and cos(SZA), the effect of ozone column is considered but the effect of temperature is not considered. By fitting the relationship at different ozone classes (classification width=30DU), we found that ozone column increasing by 30DU results in $j(O^1D)$ at a constant SZA and AOD decreasing by 18%. Therefore, the parametric equation for $j(O^1D)$ is transformed into the form E6, which reflects the influence of ozone column. The parameters a_1-a_6 correspond to ozone column range = 300-330 DU, thus we use 315 DU as the weighted standard of ozone column. The fitting parameters a_1-a_6 for $j(O^1D)$ is shown in Table 6.

Line 483-486: The coefficients of determination of the fitting equations are greater than 0.95 for $j(NO_2)$ and $j(O^1D)$ at a certain O_3 column, indicating that both of the photolysis frequencies strongly depended on AOD and cos(SZA),

Line 493-498: According to the parametric equations, aerosols lead to a decrease in seasonal mean $j(NO_2)$ by 24% and 30% and a decrease in seasonal mean $j(O^1D)$ by 27% and 33% in summer and winter under clear-sky conditions, respectively, compared to an aerosol-free atmosphere. The decreasing ratio of the photolysis frequencies in winter is higher than in summer mainly due to the higher SZA in winter.

Line 511-512: The result of Hodzic et al. (2007) is comparable with the reduction ratio of this study possibly due to the equivalent levels of AOD and SSA.

Line 518-520:

Line 547-549: Figure 8. Since the decreasing amplitude of the daytime ozone production rate is far larger than that of the daytime ozone loss rate, the mean daytime net production rate of ozone is reduced by 25%.

Line 635-637: this result was probably related to a higher proportion of scattering

aerosols under high AOD conditions than under low AOD conditions.

Line 641-645: According to the parametric equation, aerosols lead to a decrease in seasonal mean j(NO_2) by 24% and 30% for summer and winter, respectively, and the corresponding decrease in seasonal mean j(O^1D) by 27% and 33% respectively, compared to an aerosol-free atmosphere.

Line 646-647: In order to evaluate the effects of aerosols on ozone production rate, we carried out an observation campaign in August 2012.

Line 681-686:

Bais, A. F., Kazantzidis, A., Kazadzis, S., Balis, D. S., Zerefos, C. S., Meleti, C. Deriving an effective aerosol single scattering albedo from spectral surface UV irradiance measurements, ATMOSPHERIC ENVIRONMENT, 39, 1093-1102, DOI: 10.1016/j.atmosenv.2004.09.080, 2005.

Bass, A. M., Ledford, A, E,, and Laufer, A. H., Extinction coefficients of NO_2 and N_2O_4, J. Res. Nat. Bureau Standards, 80A, 143-162, 1976.

Line 711-715:

Daumont, D., Brion, J., Charbonnier, J., Malicet, J. Ozone UV spectroscopy I: absorption cross-sections at room temperature. Journal of Atmospheric Chemistry 15, 145-155, 1992.

Davenport, J.E. Determination of NO_2 photolysis parameters for stratospheric modelling, FAA Report No. FAA-EQ-7-14, 1978.

Line 723-725:

Eskes, H. J., Van Velthoven, P. F. J., Valks, P. J. M., Kelder, H. M. Assimilation of GOME total ozone satellite observations in a three-dimensional tracer transport model, Q.J.R.Meteorol.Soc. 129, 1663-1681, doi:10.1256/qj.02.14, 2003.

Line 778-779:

Harker, A. B., Ho, W., and Ratto, J. J. Photodissoclation quantum yields of NO_2 in the region 375 to 420 nm, Chem Phys. Lett. 50, 394-397, 1977.

Line 807-828:

Jones, I. T. N. and Bayes, K.D. Photolysis of nitrogen dioxide, J. Chem. Phys. 59,

4836-4844, 1973.

Kazadzis, S., Bais, A. F., Balis, D., Zerefos, C. S., and Blumthaler, M. Retrieval of down-welling UV actinic flux density spectra from spectral measurements of global and direct solar UV irradiance, J. Geophys. Res., 105, 4857-4864, 2000.

Kazadzis, S., Topaloglou, C., Bais, A. F., Blumthaler, M., Balis, D., Kazantzidis, A., Schallhart, B. Actinic flux and O^1D photolysis frequencies retrieved from spectral measurements of irradiance at Thessaloniki, Greece, ATMOSPHERIC CHEMISTRY AND PHYSICS, 4, 2215-2226, DOI: 10.5194/acp-4-2215-2004, 2004.

Kazadzis, S., Amiridis, V., and Kouremeti, N. The Effect of Aerosol Absorption in Solar UV Radiation, Advances in Meteorology, Climatology and Atmospheric Physics, 1041-1047, 2012.

Krotkov, N., Bhartia, P. K., Herman, J., Slusser, J., Scott, G., Labow, G., Vasilkov, A. P., Eck, T. F., Dubovik, O., Holben, B. N. Aerosol ultraviolet absorption experiment (2000 to 2004), part 2: Absorption optical thickness, refractive index, and single scattering albedo, OPTICAL ENGINEERING, 44, 4, 041005. DOI: 10.1117/1.1886819, 2005.

Kylling, A., Webb, A. R., Bais, A. F., Blumthaler, M., Schmitt, R., Thiel, S., Kazantzidis, A., Kift, R., Misslebeck, M., Schallhart, B., Schreder, J., Topaloglou, C., Kazadzis, S., and Rimmer, J.: Actinic flux determination from measurements of irradiance, J. Geophys. Res., 108 (D16), 4506-4515, 2003.

Line 875-882：

Matsumi, Y., Comes, F.J., Hancock, G., Hofzumahaus, A., Hynes, A.J., Kawasaki, M., Ravishankara, A.R., Quantum yields for production of $O(^1D)$ in the ultraviolet photolysis of ozone: recommendation based on evaluation of laboratory data. Journal of Geophysical Research 107 (D3), 4024. doi:10.1029/2001JD000510. 2002.

Malicet, J., Daumont, D., Charbonnier, J., Parisse, C., Chakir, A., Brion, J. Ozone UV spectroscopy. II. Absorption cross-sections and temperature dependence. Journal

of Atmospheric Chemistry 21 (3), 263-273, 1995.

Line: 924-932:

Matsumi, Y., Comes, F.J., Hancock, G., Hofzumahaus, A., Hynes, A.J., Kawasaki, M., Ravishankara, A.R., Quantum yields for production of $O(^1D)$ in the ultraviolet photolysis of ozone: recommendation based on evaluation of laboratory data. Journal of Geophysical Research 107 (D3), 4024. doi:10.1029/2001JD000510. 2002.

Malicet, J., Daumont, D., Charbonnier, J., Parisse, C., Chakir, A., Brion, J. Ozone UV spectroscopy. II. Absorption cross-sections and temperature dependence. Journal of Atmospheric Chemistry 21 (3), 263-273, 1995.

The impact of aerosols on photolysis frequencies and ozone production in urban Beijing during the four-year period 2012–2015

Wenjie Wang[1], Min Shao[1,2*], Min Hu[1], Limin Zeng[1], Yusheng Wu[1]

1 State Joint Key Laboratory of Environmental Simulation and Pollution Control, College of Environmental Sciences and Engineering, Peking University, Beijing 100871, China

2 Institute for Environmental and Climate Research, Jinan University, Guangzhou 511443, China

*** Correspondence to:**

Prof. Min SHAO

College of Environmental Sciences and Engineering, Peking University, Beijing 100871, China

Tel: +86-10-62757973; Fax: +86-10-62757973

Email: mshao@pku.edu.cn

Abstract

During the period 2012-2015, the photolysis frequencies were measured at the Peking University site (PKUERS), a representative site of urban Beijing. We present a study of the effects of aerosols on two key photolysis frequencies, $j(O^1D)$ and $j(NO_2)$. Both $j(O^1D)$ and $j(NO_2)$ display significant dependence on AOD (380nm) with a nonlinear negative correlation. With the increase in AOD, the slopes of photolysis frequencies vs AOD decrease, which indicates that the capacity of aerosols to reduce the actinic flux decreases with AOD. ~~In addition, the~~ The absolute values of slopes are equal to 4.2~~1~~-6.9~~3~~$\times10^{-6}$ s^{-1} and 3.2~~0~~$\times10^{-3}$ s^{-1} per AOD unit for $j(O^1D)$ and $j(NO_2)$ respectively at SZA of 60° and AOD smaller than 0.7, ~~both of which are larger than those observed in the Mediterranean~~ both of which are larger than those observed in a similar, previous study in the Mediterranean. This indicates that the aerosols in urban Beijing have a stronger extinction effect on actinic flux than absorptive dust aerosols in the Mediterranean. Since the photolysis frequencies strongly depended on the AOD and the solar zenith angle (SZA), we established a parametric equation to quantitatively evaluate the effect of aerosols on photolysis frequencies in Beijing. According to the parametric equation, aerosols lead to a decrease in seasonal mean $j(NO_2)$ by 24~~.2~~% and 30~~.4~~% for summer and winter, respectively, and the corresponding decrease in seasonal mean $j(O^1D)$ by 27~~.3~~% and 3~~2.6~~3% respectively, compared to an aerosol-free atmosphere (AOD = 0). Based on an observation campaign in August 2012, we used the photochemical box model to simulate the ozone production rate ($P(O_3)$). The simulation results shows that the

monthly ~~average~~ mean daytime net ozone production rate is reduced by up to 25% due to the light extinction of aerosols. Through further in-depth analysis, it was found that particulate matter concentrations maintain high level under the condition of high concentrations of ozone precursors (VOCs and NOx), which inhibits the production of ozone to a large extent. This phenomenon implies a negative feedback mechanism in the atmospheric environment of urban Beijing.

1. Introduction

Solar radiation plays an important role in atmospheric photochemistry, driving the photolysis of many key species. The photolysis of ozone (O_3), gaseous nitrous acid (HONO), and carbonyl species, which contributes to the primary production of HOx (Volkamer et al., 2010). The photolysis of ozone produces O^1D, which then reacts with H_2O to form OH radicals; these radicals are the main source of OH radicals in the troposphere, as shown by reactions R1 and R2. The strong dependence of OH concentration on $j(O^1D)$ was found in a number of field measurements (Ehhalt et al., 2000; Rohrer et al., 2014; Stone et al., 2012). In addition, the photolysis of NO_2 produces O^3P, and then O^3P reacts with O_2 to produce O_3, as shown by reactions R3 and R4, which is the only significant chemical source of ozone in the troposphere (Finlayson-Pitts et al., 2000). The photolysis frequencies of R1 and R3 are $j(O^1D)$ and $j(NO_2)$, respectively.

$$O_3 + h\nu\ (\lambda < 330\ nm) \rightarrow O^1D + O_2 \quad \text{(R1)}$$

$$O^1D + H_2O \rightarrow 2OH \quad \text{(R2)}$$

$$NO_2 + h\nu\ (\lambda < 430\ nm) \rightarrow NO + O^3P \quad \text{(R3)}$$

$$O^3P + O_2 \rightarrow O_3 \quad \text{(R4)}$$

The photolysis frequencies are calculated by the following formula:

$$j = \int_{\lambda_1}^{\lambda_2} F(\lambda)\sigma(\lambda, T)\varphi(\lambda, T)\,\mathrm{d}\lambda \quad \text{(E1)}$$

F(λ) is the actinic flux dependent on wavelength. Since the photolysis rates are proportional to the actinic flux and not all stations acquire a 2π spectroradiometer or chemical actinometers for J measurements, several methods have been developed to determine actinic flux and photolysis frequencies from ground based measurements of irradiance (Kylling et al 2003, Kazadzis et al. 2000, 2004, Topaloglou et al. 2005, Trebs et al. 2009). σ(λ, T) is the absorption cross section of the species that absorbs in the wavelength range λ_1-λ_2. φ(λ, T) is the quantum yield of the photodissociation reaction product. λ, and T represent wavelength, species and temperature, respectively.

The effect of aerosols on photolysis frequencies depends on the aerosol optical properties, SZA and altitude (Liao et al., 1999). The aerosol optical depth (AOD) characterizes the integral of the extinction coefficient of aerosols in the vertical direction. The light extinction of aerosols includes scattering and absorption, which have different effects on the actinic flux. Previous studies showed that scattering aerosols can enhance the actinic flux throughout the troposphere, while absorptive aerosols reduce the actinic flux throughout the boundary layer (Jacobson, 1998;

Dickerson et al., 1997; Castro et al., 2001; Flynn et al., 2010). To distinguish between these two components, single scattering albedo (SSA) is defined as the ratio of the scattering coefficient to the total extinction coefficient. In areas with severe aerosol pollution, aerosols can significantly affect photolysis frequencies and ozone production. Studies in Los Angeles (Jacobson, 1998), Mexico City (Castro et al., 2001; Raga et al., 2001; Li et al., 2011), São Paulo (de Miranda et al., 2005), Huston (Flynn et al., 2010), Europe (Real et al., 2011) and Russia (Pere et al., 2015) have found that aerosols reduce ozone concentration by 5-30% by attenuating photolysis frequencies. Studies in the eastern United States have shown that scattering aerosols increase ozone concentration by 5-60% by increasing the photolysis frequencies (Dickerson et al., 1997; He and Carmichael, 1999). Therefore, it is necessary to quantitatively evaluate the effect of aerosols on photolysis frequencies for a better understanding of ozone formation under highly polluted conditions.

Currently, the methods for quantitatively evaluating the influence of aerosols on photolysis frequencies mainly include radiative transfer model and parameterization method (Madronich et al., 1993). Radiative transfer model is based on an algorithm for calculating solar radiation and photolysis frequencies (Madronich et al., 1999). The observed data of related influential factors of the photolysis frequencies are taken as the model's input to calculate ~~and~~ the photolysis frequencies ~~simulated are compared with the observed value to test the simulation effect~~. This ~~The~~ method comprehensively considers the influence of aerosol optical properties on the photolysis frequencies, but it does not necessarily reflect the true quantitative

relationship in the atmosphere due to complicated environmental conditions and thus the simulated results don't necessarily reproduce observed values well (Lefer et al., 2003; Shetter et al., 2003; Hofzumahaus et al., 2004). For example, the simulated slope of $j(O^1D)$ vs AOD by Fast-JX algorithm within the CHIMERE model was significantly smaller than the observed slope, particularly for the high SZA values (Mailler et al., 2016). The parameterization method is based on the observation data taken from a certain region and is used to establish the parameterized relationship between the photolysis frequencies and optical properties of aerosols (such as AOD). The method can reflect the actual atmospheric environment conditions; it also considers less influential factors and thus is easy to apply (Casasanta et al., 2011; Gerasopoulos et al., 2012). The disadvantage of this method is that the established parametric equations apply only to a specific region and cannot be extended to other regions.

With rapid economic development and urbanization in past decades, China's atmospheric pollution has become more and more severe, characterized by high concentrations of particulate matter and ozone. Satellite observations indicates that both the particulate matter and the ozone of eastern China are at higher levels compared with other locations in the globe (Verstraeten et al., 2015; Ma et al., 2014). Levels of pollution in the Beijing–Tianjin–Hebei are even more severe (Chang et al., 2009; Che et al., 2008; Zhang et al., 2014, Zhang et al., 2016). Therefore, it is necessary to study the effects of aerosols on photolysis frequencies and ozone production in the urban areas of China.

Previous model studies have shown that aerosols in China can affect ozone production by changing the photolysis ~~rate~~frequencies. Tang et al. (2004) used a sulfur transmission–emission model (STEM) to discover that ozone concentration in northeastern China was reduced by 0.1–0.8% in the sandstorm due to the change in photolysis~~–~~ frequencies ~~rate~~. Tie et al. (2005) used a global aerosol–chemical model to show that aerosols caused $j(O^1D)$ and $j(NO_2)$ to decrease in winter by 20%-30% and 10%-30%, respectively, and in summer by 5%-20% and 1%-10%, respectively, resulting in 2%-5% and 2% reductions in ozone concentration in winter and summer, respectively. Li et al. (2011) used an air quality model to estimate the changes in the photolysis ~~rate~~ frequencies ~~–~~caused by sulfate, nitrate, ammonium, and mineral dust aerosols in the central and eastern regions of China from June 1 to June 12, 2006. This study showed that the daily average $j(O^1D)$ in the troposphere at the altitude of 1 km, 3 km, and 10 km from the ground was reduced by 53~~.3~~%, 37~~.2~~%, and 21%, respectively, resulting in a decrease in the ozone concentration by 5.4%, 3.8%, and 0.10% in the three layers. Lou et al (2014) found that with aerosols, annual mean photolysis~~–~~ frequencies ~~rates~~, $j(O^1D)$) and $j(NO_2)$, were simulated to be reduced by 6-18% in polluted eastern China, leading to reductions in O_3 of up to 0.5 ppbv in those regions in spring and summer by using the global chemical transport model (GEOS-Chem). However, all of these studies base their results on model simulations. Research using long-term observational data to evaluate the effects of aerosols on photolysis frequencies and ozone production in China has not yet been published.

Our overall goal is to quantitatively evaluate the effect of aerosols in urban

Beijing on photolysis frequencies and thus on ozone production. First, the relationship between $PM_{2.5}$ and AOD was investigated. Second, based on long-term observations (2012-2015) of photolysis frequencies, we discussed the impact of AOD on photolysis frequencies ($j(O^1D)$ and $j(NO_2)$) in urban Beijing in detail. The relationship between photolysis frequencies and AOD is adequately compared with previous study in the Mediterranean (Casasanta et al., 2011; Gerasopoulos et al., 2012). Then, the quantitative relationship between photolysis frequencies, AOD, and SZA was acquired by the parameterization method, which could be used to quantitatively evaluate the effect of AOD on photolysis frequencies in Beijing. Finally, a photochemistry box model was used to evaluate the effect of aerosols on ozone production.

2. Methodology

2.1. Measurement

From August 2012 to December 2015, $j(O^1D)$ and $j(NO_2)$ were measured continuously at PKUERS site. The data of the period during October 2012 to March 2013 and August 2015 are missed due to instrument maintenance and other measurement campaigns. The site (39.99°N, 116.31°E) is located on the sixth floor of a campus building at the Peking University, 20 km northwest of Tiananmen Square. The height from the ground is about 30 m. The sampling point is surrounded by classroom buildings. Concentration level and composition of air pollutants were thought to be similar to the downtown so as to be representative for the whole of Beijing (Wang et al., 2010; Xu et al., 2011; Zhang et al., 2012; Zhang et al., 2014).

The actinic flux was measured using a spectroradiometer and the photolysis frequencies were calculated from the absorption cross section and quantum yield of each species (Shetter and Müller~~Muler~~, 1999). The spectroradiometer consisted of a single monochromator with a fixed grating (CARL ZEISS), an entrance optic with a 2π steradian (sr) solid angle quartz diffusor and a 2048×64-pixel photodiode array detector. The spectral measurements were performed with a wavelength resolution of 2 nm, covering a wavelength range of 290-650 nm (Hofzumahaus et al., 1999). A 1000 W National Institute of Standard and Technology (NIST) traceable lamp was used for calibration under laboratory conditions (Bohn et al., 2008). The measured spectra were corrected for dark signal and stray light. For $j(O^1D)$, the quantum yields used were taken from Matsumi et al.(2002), while the ozone cross section was derived from Daumont et al. (1992) and Malicet et al. (1995). Measured temperatures were used to retrieve ozone absorption cross section and quantum yield. For $j(NO_2)$, the quantum yields used were taken from Bass et al. (1976) and Davenport et al. (1978), while the cross section was derived from Jones and Bayes (1973), Harker et al. (1977) and Davenport (1978). The calculated photolysis frequencies had a time resolution of 10 s and an accuracy of ±10% including uncertainties associated with the quartz receiver and stray-light effects (Edwards and Monks, 2003).

The optical properties of aerosols were measured by a CIMEL solar photometer (AERONET level 2 data collection, http://aeronet.gsfc.nasa.gov/) and the site selected ~~was~~ is the Beijing-CAMS site (39.93°N, 116.32°E), which is ~~close to~~6.4km

from the PKUERS site. The CIMEL solar photometer is an automatic solar-sky scanning radiometer that uses selected spectral channels. The instrumentation, data acquisition, retrieval algorithms, and calibration procedure conform to the standards of the AERONET global network and have been described in detail by Fotiadi et al. (2006). The solar extinction measurement was performed every 3 minutes in the spectral range 340–1020 nm for the calculation of AOD at wavelengths 340, 380, 440, 500, 675, 870, 970, and 1020 nm. Under cloudless conditions, the overall uncertainty of AOD data is ± 0.01 at $\lambda > 440$ nm and ± 0.02 at shorter wavelengths. In this study, AOD at the wavelength of 380 nm was chosen for analysis. This wavelength was selected as it is more representative of $j(NO_2)$. Additionally, at this wavelength we can better compare with the results of Gerasopoulos et al. (2012). The daytime clear-sky conditions were identified according to the presence of AOD data of AERONET since AOD data are unavailable under cloudy conditions. AE were also acquired from ARONET. The SSA (525nm) data were derived from a field campaign undertaken in August 2012. The absorption and scattering coefficients were measured with an Aethalometer (AE-31, Magee) and a Single Wavelength Integrating Nephelometer (Aurora-1000), respectively, with a time resolution of 1 minute. Five-minute averages of ~~ozone column concentration~~AOD, SSA, and photolysis frequencies were analyzed in this study. The total ozone column was obtained by OMI (Ozone Monitoring Instrument) for the year 2012-2015, using overpass data (http://www.temis.nl/protocols/O3global.html) (Henk et al., 2003). In addition, meteorological parameters such as temperature, relative humidity, and

pressure were simultaneously observed at this site. Table 1 presents total O_3 column, temperature, relative humidity, daytime clear-sky fraction and respective standard deviation for different seasons.

The analysis of the effects of aerosols on ozone production (Section 3.4) was based on the field campaign undertaken in August 2012. The relevant contents and methods of observation are shown in Table ~~1~~2. ~~In addition, meteorological parameters such as temperature, humidity, and pressure were simultaneously observed at the site.~~ Since the time resolution of VOCs is 1 hour, all data analyzed in Section 3.4 was processed as 1-hour average values. In this study, we focused on the effects of aerosols on photolysis frequencies and ozone production under cloudless conditions.

2.2 Radiative Transfer Model Description

We use the Tropospheric Ultraviolet and Visible (TUV) radiation model (version 5.3) provided by Sasha Madronich (Madronich, 1993). In order to solve the radiative transfer equation, TUV uses the discrete-ordinates algorithm (DISORT) with 4 streams and calculates the ~~global irradiance spectra~~ actinic flux spectra with wavelength range of 280-420 nm in 1 nm steps and resolution. Measured temperatures and ozone column were used to calculate the absorption cross sections and quantum yields. The key aerosol optical properties including AOD, SSA and AE ~~are~~ were input into the model to test the effect of aerosols on photolysis frequencies. AE(380/550nm) is taken from AERONET and the mean value of 1.3 during June 2012 - December 2015 is used in TUV model.

2.3 Photochemical box model

The photochemical box model used in this study is based on a regional atmospheric chemical mechanism (RACM2) described by Goliff et al. (2013). The mechanism includes 17 stable inorganic compounds, 4 intermediate inorganic compounds, 55 stable organic compounds, and 43 intermediate organic compounds. Compounds not specifically treated in RACM are incorporated into species with similar functional groups. The isoprene-related mechanism used in this model is LIM mechanism proposed by Peeters et al. (2009). In this study, the observed NO_2, CO, SO_2, C2–C12 NMHCs, HCHO, photolysis frequencies, temperature, pressure, and relative humidity were used as constraints to simulate the concentrations of reactive radicals (RO_2, HO_2, and OH), intermediate species, and associated reaction rate constants. HONO wasn't measured during the period and was calculated according to the concentration of NO_2 and the observed ratio of HONO to NO_2 at an urban site in Beijing, which had a marked diurnal cycle, a maximum in the early morning (ratio values up to ~0.05–0.08 in summer) and a decrease during daytime to values around 0.01–0.02 (Hendrick et al., 2014). The model was spun up for two days once it started running in order to ensure that the simulation was stable. It was assumed that the lifetime of simulated species removed by dry deposit was 24 hours. The lifetime corresponds to the assumed deposit rate of 1.2 cm s^{-1} and a well-mixed boundary layer height of about 1 km (Lu et al., 2012). Net ozone production is equal

to the reaction rate between peroxy radicals (RO_2 and HO_2) and NO minus the loss rate of NO_2 and O_3 as shown in E2, E3, and E4 as derived by Mihelcic et al. (2003). The ozone production rate ($P(O_3)$), the ozone loss rate ($D(O_3)$), and the net $P(O_3)$ were calculated from the simulation results.

$$P(O_3) = k_{HO2+NO}[HO_2][NO] + \Sigma\left(k^i{}_{RO2+NO}\left[RO^i{}_2\right][NO]\right) \quad \text{(E2)}$$

$$D(O_3) = (\theta j(O^1D) + k_{OH+O3}[OH] + k_{HO2+O3}[HO_2] + \Sigma(k^j{}_{alkene+O3}[alkene^j]))[O_3] + k_{OH+NO2}[OH][NO_2] \quad \text{(E3)}$$

$$net\ P(O_3) = P(O_3) - D(O_3) \quad \text{(E4)}$$

where θ is the fraction of O^1D from ozone photolysis that reacts with water vapor. i and j represent the number of species of RO_2 and alkenes, respectively.

3. Results and discussion

3.1 The correlation between $PM_{2.5}$ and AOD

~~In order to evaluate the extinction capacity of near-surface $PM_{2.5}$, we investigated the relationship between $PM_{2.5}$ and AOD (at 380nm).~~ Compared with AOD, $PM_{2.5}$ is a more common proxy to evaluate the level of particulate matter pollution in spite that AOD is a more closely related parameter of photolysis

frequencies. As a result, we attempted to analyze the quantitative relationship between $PM_{2.5}$ and AOD to evaluate the influence of $PM_{2.5}$ on AOD and thus on photolysis frequencies. The factors that affect this relationship include aerosol type, aerosol size distribution, aerosol distribution in the vertical direction, relative humidity (RH) and planetary boundary layer height (PBLH) (van Donkelaar et al., 2010). Figure 1 shows the correlation between AOD and $PM_{2.5}$ in four different seasons. The determination coefficient (r^2) is 0.53, 0.58, 0.62 and 0.59 for spring (March, April and May), summer (June, July and August), autumn (September, October and November) and winter (December, January and February), respectively. Meanwhile, the correlation exhibits significant seasonal differences, having relatively smaller slope (23.56) in summer and relatively larger slope (73.76) in winter. This implies that $PM_{2.5}$ in summer has stronger light extinction capacity than in winter. One reason for the seasonal differences is the variation in RH among different seasons (Table ~~2~~1). There is higher RH in summer (57.2% on average) than in winter (30.4% on average), leading to stronger hygroscopic growth of aerosol particles, and thus resulting in higher scattering ability of aerosol particles. According to another study in urban Beijing, the higher the RH, the smaller the slope, and the higher the PBLH, the smaller the slope (Zheng, C. W et al., 2017). In addition, the slope was smaller for scattering-dominant aerosols than for absorbing-dominant aerosols, and smaller for coarse mode aerosols than for fine mode aerosols (Zheng, C. W et al., 2017). The slopes of the correlation between AOD (at 550nm) and $PM_{2.5}$ in this study in summer and winter are equal to 42.2μg

m^{-3} and 119.2μg m^{-3}, respectively, close to that from Ma et al. (2016) (54.9μg m^{-3} and 110.5μg m^{-3}) and Xin et al. (2016) (55.2 μg m^{-3} and 93.4μg m^{-3}), but smaller significantly than that from Zheng et al. (2017) (65~74μg m^{-3} and 143~158μg m^{-3}). The differences mainly depend on the aerosol composition and size distribution at different observational sites in Beijing. Compared with other cities in North China (Tianjin, Shijiazhuang and Baoding) (Ma et al., 2016), the slope in Beijing for winter is significantly higher~~, indicating that the extinction capacity of aerosols in Beijing is weaker in winter~~. Consequently, using $PM_{2.5}$ to estimate AOD has a large uncertainty due to multiple interference factors.

3.2 Seasonal and diurnal variability of AOD and photolysis frequencies

The diurnal cycles of AOD ~~is~~ are shown in Figure 2. AOD displays obvious diurnal variation, with relatively high level at noon and low level at dawn and evening. The diurnal variation of $PM_{2.5}$ is ~~opposite~~ significantly different from ~~to~~ AOD. ~~The opposite diurnal variation of AOD and $PM_{2.5}$ is mainly due to higher development of planetary boundary layer at noon, resulting in more complete mixture of particulate matter in the vertical direction.~~ In addition, AOD has obvious seasonal differences, with the highest AOD in summer and the lowest AOD in winter. Conversely, $PM_{2.5}$ in winter (~~66.9~~42μg m^{-3}) is significantly higher than in summer (~~45.5~~35μg m^{-3}). In spite of lower $PM_{2.5}$ in summer, AOD in summer is higher due to stronger extinction capacity of $PM_{2.5}$ as discussed in 3.1. Figure 3 shows the diurnal

variation of the photolysis frequencies under cloudless conditions for each season. $j(O^1D)$ and $j(NO_2)$ are both highest in summer, followed by spring and autumn, and lowest in winter. This seasonal difference is mainly determined by the difference in SZA for the four seasons.

The observed mean daily maxima of photolysis frequencies at this site are lower than that observed in the eastern Mediterranean (Crete, Greece, 35°20′N, 25° 40′E) (Gerasopoulos et al., 2012) by $7.8\times10^{-6} \pm 5.5\times10^{-6}$ s^{-1} and $4.9\times10^{-6} \pm 1.8\times 10^{-6}$ s^{-1} for $j(O^1D)$, and $1.9\times10^{-3} \pm 1.2\times10^{-3}$ s^{-1} and $3.3\times10^{-3} \pm 1.0\times10^{-3}$ s^{-1} for $j(NO_2)$, in summer and winter respectively. The corresponding lower photolysis frequencies of Beijing than the eastern Mediterranean due to SZA difference is 1.7×10^{-6} s^{-1} and 3.0×10^{-6} s^{-1} for $j(O^1D)$, and 8.0×10^{-5} s^{-1} and 6.6×10^{-4} s^{-1} for $j(NO_2)$ according to TUV model under aerosol-free conditions, which are significantly lower than observed decreased magnitudes. Additionally, we know that the temperature is lower in Beijing during the winter compared to conditions in Crete. The measured mean temperature in Beijing during winter is equal to 0.53±4.2 ℃ (Table 1). When we consider the temperature in Crete is 10 ℃ higher than in Beijing, the lower $j(O^1D)$ of Beijing than Crete is 5.5×10^{-7} s^{-1}, which is also not able to compensate the $j(O^1D)$ gap between the two sites during winter. Taking into account the similar levels of ozone column concentration in the two sites, the large gap of photolysis frequencies in the two sites is mainly attributed to the higher AOD in Beijing (0.76±0.75) than in the eastern Mediterranean (0.27±0.13).

It can be seen from Figure 3 that the difference between winter and summer for $j(O^1D)$ is significantly larger than that for $j(NO_2)$, where the summer midday averages of $j(O^1D)$ and $j(NO_2)$ are 5 times and 2 times those of winter, respectively. There are two reasons for this phenomenon. One, compared with $j(NO_2)$, $j(O^1D)$ is more sensitive to the change in SZA and the same change in SZA results in a larger change in $j(O^1D)$ than $j(NO_2)$. Two, the main influential factors of $j(NO_2)$ under cloudless conditions are SZA and AOD, and the influence of ozone column concentration and temperature on $j(NO_2)$ is negligible. However, $j(O^1D)$ is affected significantly by the ozone column concentration and temperature, in addition to SZA and AOD. The higher ozone column concentration and lower temperature in winter than in summer lead to the difference in $j(O^1D)$ further increasing (Table ~~2~~1).

3.3 The correlation between photolysis frequencies and AOD

3.3.1 The correlation between $j(O^1D)$ and AOD

In order to rule out the effect of SZA on photolysis frequencies, we chose SZA equal to 30° and 60° (± 1°) for analysis. Figure 4 presents the dependence of $j(O^1D)$ on AOD at different levels of ozone column concentration at SZA of 30° and 60° (± 1°). The ozone column concentration has a classification width of 30 DU. This relatively large classification width is chosen to make sure that there are enough points to fit the relationship between $j(O^1D)$ and AOD. $j(O^1D)$ exhibits a clear

dependence on AOD, with a nonlinear negative correlation. The scatter of these points is mainly due to variations in ozone column and temperature. As AOD increased, the slope of $j(O^1D)$-AOD gradually decreases, indicating that the ability of aerosols to reduce $j(O^1D)$ gradually decreases with AOD. This result differs from that found in Mediterranean, where $j(O^1D)$ was linearly negatively correlated with AOD (Casasanta et al., 2011; Gerasopoulos., 2012). A larger variation range of AOD in Beijing (0-3) compared with Mediterranean (0-0.6) is one reason for the difference.

For further analysis, the observed relation between $j(O^1D)$ and AOD was compared with TUV-simulated results. Panels a and b of Figure 5 present the comparison between observed and TUV-simulated $j(O^1D)$ against AOD at a SZA of 30° and 60° respectively and ozone column concentration of 330-360 DU. The observed $j(O^1D)$ was at ozone column of 330-360DU and were scaled to the temperature of 298K. AE(380/550nm) = 1.3, ozone column = 345 and Temperature = 298K were used in TUV model for all simulations. Mean Earth-Sun distance was used in the calculations of TUV model and measured j-values were scaled to the mean Earth-Sun distance. At low AOD level (< 0.8), the observed slope of $j(O^1D)$ vs AOD is significantly larger than the simulated slope at SSA of 0.95, and slightly larger than the simulated slope at SSA of 0.85. With AOD increasing, the observed slope decreases rapidly to the level smaller than the simulated slopes. The rapid change of the slope with AOD can be related to the variation of SSA at different AOD level. Figure 6 presents the relationship between SSA and AOD based on

observed data in August 2012. The result suggests a significant correlation between SSA and AOD. With the increase in AOD, SSA is elevated; meanwhile, the slope of SSA vs AOD is gradually reduced. Similar results in other regions have been obtained by Bais et al., 2005, Krotkov et al., 2005 and Kazadzis et al., 2012). SSA characterizes the ratio of the scattering extinction coefficient to the total extinction coefficient (scattering extinction coefficient plus absorptive extinction coefficient) of aerosols. The smaller the SSA, the higher the absorptive component and lower the scattering component of the aerosol, and the stronger the ability of the aerosol to reduce the actinic flux (Dickerson et al., 1997). Figure 6 indicates that aerosols in Beijing under low AOD conditions had a higher proportion of absorptive aerosol components than under high AOD conditions, and, as a result, had a stronger ability to reduce the photolysis frequencies, which contributed to the rapidly reduced slope of $j(O^1D)$ vs AOD with AOD. However, due to absence of more SSA data of the period 2012-2015, we can't give more sufficient evidence for the dependence of SSA on AOD. For another perspective, Owing to the biomass burning and soot emission generated from heating, the fine mode heavily-absorbing aerosol percentage is higher in winter than in summer (Zheng et al., 2017; Liu et al., 2016; Zhang et al., 2013), and thus aerosols in winter have stronger ability to reduce the photolysis frequencies. High AOD levels often appeared in summer and low AOD levels occurred mostly in winter (Figure 2), another fact that may also explains the rapidly reduced slope of $j(O^1D)$ vs AOD with AOD.

Comparing panels a and b of Figure 4, we see that at AOD smaller than 1, the slope of $j(O^1D)$ vs AOD exhibits a significant dependence on SZA and the slope at 30° of SZA is about 1.5-2.0 times larger than that at 60° of SZA. This result is similar to that of the observations made in the central Mediterranean (Casasanta et al., 2011). For the purpose of comparison with the study in the Mediterranean, the slope of $j(O^1D)$ vs AOD was calculated at AOD smaller than 0.7.

Table 3 presents slope, intercept and the determination coefficient (r^2) of linear fits of correlation between $j(O^1D)$ and AOD for each ozone column class at AOD smaller than 0.7. At SZA of 60° and O_3 column concentration of 300-330 DU, the respective slope of the linear regression indicates a reduction of $j(O^1D)$ by $4.2\underline{1}\times10^{-6}$ s^{-1} per AOD unit. Gerasopoulos et al. (2012) reported that the observed slope in the eastern Mediterranean was equal to $2.4\underline{4}\times10^{-6}$ s^{-1} at O_3 column of 300-320 DU. Casasanta et al. (2011) reported that the observed slope in the central Mediterranean varied from $2.66\underline{7}\times10^{-6}$ s^{-1} to $3.87\underline{9}\times10^{-6}$ at O_3 column of 300-330 DU. All of these results are smaller than the value of the present study, indicating that aerosols in urban Beijing had a stronger extinction capacity on $j(O^1D)$ than those in the Mediterranean that was influenced by both natural absorptive aerosols and anthropogenic aerosols. Previous study indicated that SSA in Beijing ranged from 0.80 to 0.86 (Garland et al., 2009;Han et al., 2015b; Han et al., 2017; Tian et al., 2015). The relatively low SSA in Beijing could be an important reason for the stronger extinction capacity.

3.3.2 The correlation between $j(NO_2)$ and AOD

Unlike $j(O^1D)$, $j(NO_2)$ is negligibly affected by ozone column concentration and depends mainly on AOD and SZA under cloudless conditions. Figure 7 presents the dependence of $j(NO_2)$ on AOD at different SZA levels under cloudless conditions. The cosine of SZA (cos (SZA)) is categorized according to a width of 0.2. In the same category of cos (SZA), $j(NO_2)$ displays a strong dependence on AOD. The scatter of these points is due to the relatively large classification width of SZA to a large extent. When cos(SZA) is at its maximum level (0.8-1), the correlation between $j(NO_2)$ and AOD is close to linear. When cos (SZA) decreases, the correlation tends to be nonlinear. Similar to $j(O^1D)$, the observed slopes of $j(NO_2)$ vs AOD are also larger than TUV-simulated slope at SSA of 0.95 and 0.85 when AOD is smaller than 0.8, and decreased rapidly with increasing AOD (panels c and d of Figure 5). The reason for this result is the same with that for $j(O^1D)$ as explained above.

Table 4 presents the slope, intercept and the determination coefficient (r^2) of linear fits of correlation between $j(NO_2)$ and AOD for each ozone column class at AOD smaller than 0.7. The slope of $j(NO_2)$ vs AOD also displays a significant dependence on cos(SZA). The slope increases as cos(SZA) increases from 0 to 0.5 and then decreases as cos(SZA) increases from 0.5 to 1. At SZA of 60°±1 (cos(SZA)=0.5±0.015), the respective slope of the linear regression indicates a

457 reduction of $j(NO_2)$ by $3.2 \cdot 10^{-3}$ s^{-1} per AOD unit. This result is larger than the value

458 for non-dust aerosols ($2.2 \cdot 10^{-3}$ s^{-1}) and close to the value for dust aerosols ($3.1 \cdot 10^{-3}$

459 s^{-1}) in the eastern Mediterranean reported by Gerasopoulos et al. (2012).

460

461 **3.4 The parameterization relationship between photolysis frequencies, AOD,**

462 **and SZA**

463

464 As analyzed above, the photolysis frequencies ($j(O^1D)$ and $j(NO_2)$) strongly

465 depended on AOD and cos(SZA) and could be fit into expression E5 using a

466 quadratic polynomial form. The fitting parametric equations for $j(NO_2)$ is shown in

467 Table 5. For $j(O^1D)$, both of O_3 column and temperature affect $j(O^1D)$ significantly.

468 Figure S1 presents the dependence of $j(O^1D)$ on ozone column at low AOD level

469 (AOD<0.3) and SZA of (a) 30°±1° and (b) 60°±1°, respectively. Ozone column

470 ranging from 270 to 400 DU leads to $j(O^1D)$ reducing about 50%. In order to

471 evaluate the impact of temperature on $j(O^1D)$, we calculated the ratio of $j(O^1D)$ at

472 measured temperature to $j(O^1D)$ at temperature = 298K ($j(O^1D)/ j(O^1D)_{T=298K}$)

473 (Figure S2). $j(O^1D)/j(O^1D)_{T=298K}$ varied from 0.82 to 1.03 indicating that temperature

474 changed $j(O^1D)$ by no more than 21%. Therefore, temperature played a minor role in

475 changing $j(O^1D)$ compared with ozone column. As a result, when we fitted the

476 relationship among $j(O^1D)$, AOD and cos(SZA), the effect of ozone column is

477 considered but the effect of temperature is not considered. By fitting the relationship

at different ozone classes (classification width=30DU), we found that ozone column increasing by 30DU results in j(O^1D) at a constant SZA and AOD decreasing by 18%. Therefore, the parametric equation for j(O^1D) is transformed into the form E6, which reflects the influence of ozone column. The parameters a_1-a_6 correspond to ozone column range = 300-330 DU, thus we use 315 DU as the weighted standard of ozone column. The fitting parameters a_1-a_6 for j(O^1D) is shown in Table 6.

$$j(NO_2) = a_1 + a_2 AOD + a_3 cos(SZA) + a_4 (AOD)^2 + a_5 AOD cos(SZA) + a_6 (cos(SZA))^2 \quad \text{.....E5}$$

$$j(O^1D) = [a_1 + a_2 AOD + a_3 cos(SZA) + a_4 (AOD)^2 + a_5 AOD cos(SZA) + a_6 (cos(SZA))^2] \times [1+(315 - O_3 \text{ column}) \times 0.006] \quad \text{……E6}$$

~~Table 5 and Table 6 presents the fitting parametric equations and the corresponding coefficients of determination (R^2) at different O_3 column ranges.~~ The coefficients of determination of the fitting equations are greater than 0.95 for j(NO_2) and j(O^1D) at a certain O_3 column, indicating that both of the photolysis frequencies strongly depended on AOD and cos(SZA) ~~at a certain O_3 column~~, and the effect of other factors such as SSA and AE are integrated into the constant term in the parametric equation. Since the ozone column concentration has greater influence on j(O^1D) than on j(NO_2), the parameters of fitting equations for j(NO_2) are similar, but the parameters of fitting equations for j(O^1D) have a large fluctuation at different O_3 column ranges (especially a_1 and a_2). The parametric equations can be used to quantitatively evaluate the effect of AOD on photolysis frequencies in Beijing.

According to the parametric equations, aerosols lead to a decrease in seasonal mean $j(NO_2)$ by 24.2% and 30.4% and a decrease in seasonal mean $j(O^1D)$ by 27.3% and 32.63% in summer and winter under clear-sky conditions, respectively, compared to an aerosol-free atmosphere. The decreasing ratio of the photolysis frequencies in winter is higher than in summer mainly due to the higher SZA ~~and lower SSA~~ in winter.

The effect of aerosols on photolysis frequencies in Beijing is compared with other studies. Real and Sartelet (2011) reported a reduction in $j(NO_2)$ and $j(O^1D)$ of 13%-14% due to aerosols by using the radiative transfer code Fast-J during summer 2001 over European regions. Flynn et al (2010) reported that aerosols reduced $j(NO_2)$ by 3% in Huston during 2006 by using TUV model. Gerasopoulos et al (2012) reported that aerosols reduced $j(NO_2)$ and $j(O^1D)$ by 5%-15% with 5-yr mean AOD at 380nm equal to 0.27. All of these results are lower than the reduction ratio of this study mainly due to higher aerosol level in Beijing (4-yr mean AOD equal to 0.76± 0.75). Hodzic et al. (2007) simulated a 15–30% $j(NO_2)$ photolysis reduction during the 2003 European summer heatwave in the case of absorbing biomass burning aerosols with AOD at 550 nm equal to 0.7-0.8 and SSA at 532 nm equal to 0.83-0.87. The result of Hodzic et al. (2007)~~this study~~ is comparable with the reduction ratio of this study possibly due to the equivalent levels of AOD and SSA. In addition, Péré et al (2015) simulated a higher reduction (20–50%) in $j(NO_2)$ and $j(O^1D)$ along the transport of the aerosol plume during the 2010 Russian summer wildfires episode.

The higher reduction is due to the higher level of AOD (peak value of AOD at 400nm reached 2-4), even though SSA is very high (0.97).

~~The above established parametric relationship of $PM_{2.5}$-AOD and $j(NO_2)$-AOD-SZA gives us a chance to estimate the effect of $PM_{2.5}$ on photolysis frequencies due to aerosol light extinction.~~

3.5 The influence of AOD on ozone production

In order to explain the effect of aerosol light extinction on ozone production, we used the data from the field observation campaign undertaken in August 2012. Ozone production depends on its precursors (NOx and VOCs), meteorological factors, and solar radiation. Solar radiation is the driving force for tropospheric photochemical reactions, in which $j(O^1D)$ and $j(NO_2)$ are both important for ozone production. On the one hand, the increase in $j(NO_2)$ promotes the photolysis of NO_2, thereby accelerating the formation of ozone. On the other hand, the increase in $j(O^1D)$ accelerates the photolysis of ozone. In addition, the increase in the photolysis frequencies will accelerate the photolysis of OVOC (especially formaldehyde and acetaldehyde), HONO, and H_2O_2, resulting in increases in OH and HO_2, which will promote the reaction between OH and VOCs and thus produce more RO_2. As a result, more ozone is produced by increasing the reaction rate between RO_2 (or HO_2) and NO. However, the increase in OH and HO_2 also consumes ozone and NO_2, which

contributes to the increase in $D(O_3)$. In brief, the overall effect of changes in photolysis frequencies on sources and sinks of ozone determines the change in the net ozone production rate.

Ozone production (HO_2 + NO, RO_2 + NO), ozone loss (O^1D + H_2O, HO_2 + O_3, O_3 + OH, NO_2 + OH, and O_3 + alkenes), and net ozone production rate during August 2012 were calculated by using the box model. We used the observed photolysis frequencies (i.e. j_obs) and the calculated photolysis frequencies by parametric equation under the condition of AOD equal to 0 (i.e. j_AOD=0), were used to constrain the box model. The difference of simulated results in the two scenarios can be attributed to the effect of aerosol light extinction. As a result, the presence of aerosols causes a decrease in both ozone production rate and loss rate, as is shown in Figure 8. Since the decreasing amplitude of the daytime ozone production rate is far larger than that of the daytime ozone loss rate, the mean daytime net production rate of ozone is reduced by 25%. This reduction is comparable with the results of the study in Mexico City, where aerosols caused a 20% reduction in the ozone concentrations (Castro et al., 2001). Studies in Houston and Crete have shown that aerosols cause ozone production rates to decrease by about 4% and 12%, respectively, which are lower than that found in this study (Flynn et al., 2010; Gerasopoulos et al., 2012).

The ratio of the observed photolysis frequencies to the photolysis frequencies at AOD equal to 0 is defined as JIF (Flynn et al., 2010). A JIF of less than 1 indicates that the aerosols cause a decrease in the photolysis frequencies. Figure 9 shows the

relation between $P(O_3)_{j\_obs}/P(O_3)_{j\_AOD=0}$ (or $D(O_3)_{j\_obs}/D(O_3)_{j\_AOD=0}$) and JIF. The majority of JIF values were less than 1, with an average of 0.72, indicating that aerosols greatly attenuated photolysis frequencies due to high levels of AOD (average of 1.07) and low levels of SSA (average of 0.84) during the observation period. $P(O_3)_{j\_obs}/P(O_3)_{j\_AOD=0}$ and $D(O_3)_{j\_obs}/D(O_3)_{j\_AOD=0}$ are both linearly positively correlated with JIF and the scatters are mostly above the 1:1 line. As can be seen from the figure 9, a 30% reduction in photolysis frequencies (JIF = 0.7) due to the presence of aerosols results in a decrease in ozone production rate and loss rate by about 26% and 15%, respectively. The decreasing amplitude in the ozone production rate is greater than the decrease in the ozone loss rate because the corresponding processes of ozone production are all light-driven, but the corresponding processes of ozone loss are not all light-driven because the reaction of O_3 with alkenes does not depend on solar radiation. According to the simulated results, the reaction of ozone with alkenes during this campaign accounts for 17% of total ozone loss.

The diurnal profile of the mean ozone production and loss rate is shown in Figure 10. $P(O_3)$ peak midday in the 12:00-14:00 local hours at 31 ppb/h without aerosol impact and 23 ppb/h with aerosol impact. The maximum $D(O_3)$ also occurrs between 12:00 and 14:00 at 4.2 ppb/h without aerosol impact and 3.5 ppb/h with aerosol impact. There is little difference between aerosol-impact and aerosol-free $P(O_3)$ (or $D(O_3)$) in the hours of 6:00-11:00, but the difference in the afternoon (12:00-18:00) is large, indicating that the reduction effect of aerosol on ozone

587 production mainly occurs during the afternoon.

588 The above analysis focuses on the effect of aerosol on the ozone production due
589 to aerosol light extinction. However, it does not consider the close relationship
590 between aerosol and ozone's gaseous precursors in the actual atmosphere. To explain
591 this problem, we chose two adjacent days (small SZA effect) with obviously
592 different AOD levels: a clean day (A day: August 21, 2012; AOD = 0.21, $PM_{2.5}$=21.6
593 $\mu g\ m^{-3}$) and a day with high aerosol pollution (B day; August 26, 2012; AOD = 3.2,
594 $PM_{2.5}$=125.0 $\mu g\ m^{-3}$) (Table 7). The difference in AOD between the two days can be
595 taken to represent the maximum daytime gap of AOD for this month. The ozone
596 column concentrations for these two days were 302 DU and 301 DU, respectively, of
597 which the effect on $j(O^1D)$ is negligible. Under these conditions, the $j(O^1D)$ value at
598 noon time decreases from $3.23 \times 10^5\ s^{-1}$ on A day to $1.29 \times 10^5\ s^{-1}$ on B day (i.e., a 60%
599 reduction) and the $j(NO_2)$ value at noon time decreases from $8.26 \times 10^{-3}\ s^{-1}$ on A day
600 to $4.19 \times 10^{-3} s^{-1}$ on B day (i.e., a 49.2% reduction). As shown in Table 7, B day has
601 higher AOD and higher concentrations of gaseous pollutants. The concentrations of
602 CO, NO_2, HCHO and the OH reactivity of VOCs in B day are much higher than in A
603 day, with the ratio of 3.6, 2.3, and 2.0, respectively. The simultaneous increases of
604 gaseous pollutants and AOD are due to the fact that gaseous pollutants (NOx, SO_2,
605 and VOCs) emitted by major pollution sources in Beijing, including traffic and
606 industry, have undergone the processes of gas-phase oxidation and nucleation to
607 generate secondary particulate matter that contributes to aerosol light extinction.
608 Previous studies have reported that secondary particulate matter has accounted for

609 more than 60% of total particulate matter during severe smog pollution in Beijing
610 summers (Han et al., 2015a; Guo et al., 2014). In addition, several studies have
611 shown that secondary components in particulate matter (especially secondary
612 organics and ammonium sulfate) have dominated the aerosol light extinction (Han et
613 al., 2014; Han et al., 2017; Wang et al., 2015). Observations made in Beijing during
614 the summer of 2006 showed that ammonium sulfate and ammonium nitrate
615 contributed 44.6% and 22.3%, respectively, to the total extinction coefficient during
616 a severe period of smog (Han et al., 2014); in the summer of 2014 in Beijing,
617 ammonium sulfate, secondary organic aerosols, and ammonium nitrate contributed
618 30%, 22%, and 18%, respectively, to the total extinction coefficient (Han et al.,
619 2017).

620 As shown in Figure 11, the simulation results indicate that the net $P(O_3)$ of B
621 day is 36.2% higher than that of A day due to higher concentrations of ozone
622 precursors on B day. This result is consistent with the observed ozone concentrations,
623 of which the observed ozone concentration in B day is 2.2 times higher than that of
624 A day. If we adjust the photolysis frequencies level of B day to the level of A day, the
625 net $P(O_3)$ increases by 70.0%, which indicates that the high level of particulate
626 matter in B day greatly inhibits ozone production. This result means that the system
627 is under negative feedback, thus keeping O_3 at a relatively stable level. Table 8
628 summarizes the average levels of gaseous pollutants and photolysis frequencies for
629 AOD less than 1 and greater than 1, as measured during August 2012. It shows that,
630 the concentrations of ozone's precursors are higher and the photolysis frequencies

631 are lower at high AOD levels (AOD > 1) than those at low AOD level (AOD < 1).
632 This result means that the negative feedback mechanism is prevalent throughout the
633 whole campaign period. Therefore, the prevention and control measures of air
634 pollution in Beijing need to incorporate this coupling mechanism between particulate
635 matter and ozone to achieve effective control of these two main pollutants.

636 **4. Conclusion**

637 Photolysis reactions are important driving forces for tropospheric
638 photochemical oxidation processes and ozone production. In this study, we explored
639 in detail the effects of aerosols on photolysis frequencies and ozone production in
640 Beijing, based on a long observation period of 4 years. We have found that:

641 (1) There is a strong correlation between $PM_{2.5}$ and AOD, and the slope in
642 summer is smaller significantly than in winter, which indicates that aerosols
643 in summer have a more efficient extinction capacity than in winter.

644 (2) As AOD increased, the extinction effect of aerosol on photolysis
645 frequencies was decreased; this result was probably related to a higher
646 proportion of scattering aerosols under high AOD conditions than under low
647 AOD conditions. The slope of the correlation between photolysis
648 frequencies and AOD indicates that the aerosols in urban Beijing have a
649 stronger extinction on actinic flux than absorptive dust aerosols in the
650 Mediterranean.

(3) The influence of AOD on photolysis frequencies was evaluated quantitatively by establishing parametric equations. According to the parametric equation, aerosols lead to a decrease in seasonal mean $j(NO_2)$ by 24~~.2~~% and 30~~.4~~% for summer and winter, respectively, and the corresponding decrease in seasonal mean $j(O^1D)$ by 27~~.3~~% and 3~~2.63~~% respectively, compared to an aerosol-free atmosphere.

(4) In order to evaluate the effects of aerosols on ozone production rate, we carried out an observation campaign in August ~~20142012~~. The results show that aerosols reduced the net ozone production rate by 25% by reducing the photolysis frequencies. High concentrations of ozone gaseous precursors were often accompanied by high concentrations of particulate matter, which, to a large extent, inhibited excessive levels of ozone generation and reflected the negative feedback effect of the atmospheric system. Therefore, the influence of aerosol on photolysis frequencies and thus on the rate of oxidation of VOCs and NOx to ozone and secondary aerosol is important for determining the atmospheric effects of controlling the precursor emissions of these two important air pollutants (aerosols and ozone).

Author contribution

Author	Contribution
Wenjie Wang	acquisition of data; analysis and interpretation of data; drafting the article and revising it critically

Min Shao	substantial contributions to conception and design; revising the article critically
Min Hu	collection of data
Limin Zeng	collection of data
Yusheng Wu	collection of data

ACKNOWLEDGEMENTS

This work was supported by the Major Program of the National Natural Science Foundation of China [Grant number 91644222]. We thank Hongbin Chen and Philippe Goloub for data management of AOD and other aerosol optical properties on AERONET.

Reference

Barnarda, J. C., Chapmana E G., Fasta, J. D., Schmelzera, J. R., Slusserb, J. R., Shetterc, R. E.: An evaluation of the FAST-Jphotolysis algorithm for predicting nitrogen dioxide photolysis rates under clear and cloudy sky conditions,

ATMOSPHERIC ENVIRONMENT, 38, 3393-3403, 10.1016/j.atmosenv.2004.03.034, 2004.

Bais, A. F., Kazantzidis, A., Kazadzis, S., Balis, D. S., Zerefos, C. S., Meleti, C. Deriving an effective aerosol single scattering albedo from spectral surface UV irradiance measurements, ATMOSPHERIC ENVIRONMENT, 39, 1093-1102, DOI: 10.1016/j.atmosenv.2004.09.080, 2005.

Bass, A. M., Ledford, A, E,, and Laufer, A. H., Extinction coefficients of NO_2 and N_2O_4, J. Res. Nat. Bureau Standards, 80A, 143-162, 1976.

Bohn, B., Corlett, G. K., Gillmann, M., Sanghavi, S., Stange, G., Tensing, E., Vrekoussis, M., Bloss, W. J., Clapp, L. J., Kortner, M., Dorn, H. P., Monks, P. S., Platt, U., Plass-Dulmer, C., Mihalopoulos, N., Heard, D. E., Clemitshaw, K. C ., Meixner, F. X., Prevot, A. S. H., Schmitt, R.: Photolysis frequency measurement techniques: Results of a comparison within the ACCENT project, ATMOSPHERIC CHEMISTRY AND PHYSICS, 8, 5373–5391, doi:10.5194/acp-8-5373-2008, 2008.

Casasanta, G., di Sarra, A., Meloni, D., Monteleone, F., Pace, G., Piacentino, S., Sferlazzo, D.: Large aerosol effects on ozone photolysis in the Mediterranean, ATMOSPHERIC ENVIRONMENT, 45, 3937-3943, 10.1016/j.atmosenv.2011.04.065, 2011.

Castro, T., Madronich, S., Rivale, S., Muhlia, A., Mar, B.: The influence of aerosols on photochemical smog in Mexico City, ATMOSPHERIC ENVIRONMENT, 35, 1765-1772, 10.1016/S1352-2310(00)00449-0, 2001.

Chang, D, Song, Y, Liu, B.: Visibility trends in six megacities in China 1973–2007, ATMOSPHERIC RESEARCH, 94, 161-167, 10.1016/j.atmosres.2009.05.006, 2009.

Che, H., Zhang, X., Li, Y., Zhou, Z., Qu, J. J., Hao, X.: Haze trends over the capital cities of 31 provinces in China, 1981–2005, THEORETICAL AND APPLIED CLIMATOLOGY, 97, 235-242, 10.1007/s00704-008-0059-8, 2009.

de Miranda, R., Andrade, M. F., Fattori, A. P.: Preliminary studies of the effect of

719 aerosols on nitrogen dioxide photolysis rates in the city of Sao Paulo, Brazil.
720 ATMOSPHERIC RESEARCH, 75, 135–148, 10.1016/j.atmosres.2004.12.004,
721 2005.
722 Daumont, D., Brion, J., Charbonnier, J., Malicet, J. Ozone UV spectroscopy I:
723 absorption cross-sections at room temperature. Journal of Atmospheric
724 Chemistry 15, 145-155, 1992.
725 Davenport, J.E. Determination of NO_2 photolysis parameters for stratospheric
726 modelling, FAA Report No. FAA-EQ-7-14, 1978.
727 Dickerson, R. R., Kondragunta, S., Stenchikov, G., Civerolo, K. L., Doddridge, B. G.,
728 Holben, N.: The impact of aerosols on solar ultraviolet radiation and
729 photochemical smog, Science, 278, 827–830, 10.1126/science.278.5339.827,
730 1997.
731 Ehhalt, D. H., Rohrer, F.: Dependence of the OH concentration on solar UV,
732 JOURNAL OF GEOPHYSICAL RESEARCH-ATMOSPHERES, 105,
733 3565-3571, 10.1029/1999JD901070, 2000.
734 Eskes, H. J., Van Velthoven, P. F. J., Valks, P. J. M., Kelder, H. M. Assimilation of
735 GOME total ozone satellite observations in a three-dimensional tracer transport
736 model, Q.J.R.Meteorol.Soc. 129, 1663-1681, doi:10.1256/qj.02.14, 2003.
737 Finlayson-Pitts, B. J., Pitts, J. N.: Chemistry of the Upper and Lower Atmosphere.
738 Academic Press, New York, 2000.
739 Flynn, J., Lefer, B., Rappenglück, B., Leuchner, M., Perna, R., Dibb, J., Ziemba, L.,
740 Anderson, C., Stutz, J., Brune, W., Ren, X. R.: Impact of clouds and aerosols on
741 ozone production in Southeast Texas. ATMOSPHERIC ENVIRONMENT, 44,
742 4126–4133, 10.1016/j.atmosenv.2009.09.005, 2010.
743 Fotiadi, A., Hatzianastassiou, N., Drakakis, E., Matsoukas, C., Pavlakis, K. G.,
744 Hatzidimitriou, D., Gerasopoulos, E., Mihalopoulos, N., Vardavas, I.: Aerosol
745 physical and optical properties in the eastern Mediterranean Basin, Crete, from
746 Aerosol Robotic Network data, ATMOSPHERIC CHEMISTRY AND PHYSICS,
747 6, 5399–5413, 10.5194/acp-6-5399-2006, 2006

748 Gao W, Tie X X, Xu J M, Huang R J, Mao X Q, Zhou G Q, Luyu Chang. Long-term
749 trend of O3 in a mega City (Shanghai), China: Characteristics, causes, and
750 interactions with precursors. SCIENCE OF THE TOTAL ENVIRONMENT, 603,
751 425–433, 10.1016/j.scitotenv.2017.06.099, 2017.
752 Garland, R.; O. Schmid, A.; Nowak, P.; Achtert, A.; Wiedensohler, S.; Gunthe, N.;
753 Takegawa, K.; Kita, Y.; Kondo, and M. Hu (2009), Aerosol optical properties
754 observed during Campaign of Air Quality Research in Beijing 2006
755 (CAREBeijing-2006): Characteristic differences between the inflow and
756 outflow of Beijing city air, JOURNAL OF GEOPHYSICAL
757 RESEARCH-ATMOSPHERES, 114, D00G04, 10.1029/2008JD010780, 2009.
758 Gerasopoulos, E., Kazadzis, S., Vrekoussis, M., Kouvarakis, G., Liakakou, E.,
759 Kouremeti, N., Giannadaki, D., Kanakidou, M., Bohn, B., Mihalopoulos, N.:
760 Factors affecting O_3 and NO_2 photolysis frequencies measured in the eastern
761 Mediterranean during the five-year period 2002–2006, JOURNAL OF
762 GEOPHYSICAL RESEARCH-ATMOSPHERES, 117, D22305,
763 10.1029/2012JD017622, 2012.
764 Goliff, W. S., Stockwell, W. R., Lawson, C. V.: The regional atmospheric chemistry
765 mechanism, version 2, ATMOSPHERIC ENVIRONMENT, 68, 174–185,
766 10.1016/j.atmosenv.2012.11.038, 2013.
767 Guo, S., Hu M, Zamora, M. L., Peng, J. F., Shang, D. J., Zheng, J., Du, Z. F., Wu, Z.
768 J., Shao, M., Zeng, L. M., Molina, M. J., Zhang, R. Y.: Elucidating severe urban
769 haze formation in China, PROCEEDINGS OF THE NATIONAL ACADEMY
770 OF SCIENCES OF THE UNITED STATES OF AMERICA, 111, 17373–17378,
771 10.1073/pnas.1419604111, 2014.
772 Han, T. T., Liu, X. G., Zhang, Y. H., Qu, Y.,Gu, J. W., Ma, Q., Lu, K. D., Tian, H. Z,,
773 Chen, J., Zeng, L. M.: Characteristics of aerosol optical properties and their
774 chemical apportionments during CAREBeijing 2006, AEROSOL AND AIR
775 QUALITY RESEARCH,14: 1431-1442, 10.4209/aaqr.2013.06.0203, 2014.
776 Han, T. T., Xu, W. Q., Chen, C., Liu, X. G., Wang, Q. Q., Li, J., Zhao, X. J., Du, W.,

Wang, Z. F., Sun, Y. L.: Chemical apportionment of aerosol optical properties during the Asia-Pacific Economic Cooperation summit in Beijing, China, JOURNAL OF GEOPHYSICAL RESEARCH-ATMOSPHERES, 120, 10.1002/2015JD023918, 2015b.

Han, T. T., Xu, W. Q., Li, J., Freedman, A., Zhao, J., Wang, Q. Q., Chen, C., Zhang, Y. J., Wang, Z. F., Fu, P. Q.: Aerosol optical properties measurements by a CAPS single scattering albedo monitor: Comparisons between summer and winter in Beijing, China, JOURNAL OF GEOPHYSICAL RESEARCH-ATMOSPHERES, 122, 2513-2526, 10.1002/2016JD025762, 2017.

Han, T., Liu, X., Zhang, Y., Qu, Y., Zeng, L., Hu, M., Zhu, T.: Role of secondary aerosols in haze formation in summer in the Megacity Beijing, JOURNAL OF ENVIRONMENTAL SCIENCES, 31, 51-60, 10.1016/j.jes.2014.08.026, 2015a.

Harker, A. B., Ho, W., and Ratto, J. J. Photodissoclation quantum yields of NO_2 in the region 375 to 420 nm, Chem Phys. Lett. 50, 394-397, 1977.

He, S., Carmichael, G. R.: Sensitivity of photolysis rates and ozone production in the troposphere to aerosol properties, JOURNAL OF GEOPHYSICAL RESEARCH-ATMOSPHERES, 104, 26307–26324, 10.1029/1999JD900789, 1999.

Hendrick, F; Muller, JF; Clemer, K; Wang, P; De Maziere, M; Fayt, C; Gielen, C; Hermans, C; Ma, JZ; Pinardi, G ; Stavrakou, T; Vlemmix, T; Van Roozendael, M., Four years of ground-based MAX-DOAS observations of HONO and NO_2 in the Beijing area. ATMOSPHERIC CHEMISTRY AND PHYSICS, 14(2), 765-781, 2014.

Hodzic, A., Madronich, S., Bohn, B., Massie, S., Menut, L., and Wiedinmyer, C.: Wildfire particulate matter in Europe during summer 2003: meso-scale modeling of smoke emissions, trans-port and radiative effects, ATMOSPHERIC CHEMISTRY AND PHYSICS, 7, 4043–4064, 10.5194/acp-7-4043-2007, 2007.

Hofzumahaus, A., Kraus, A., Muller, M.: Solar actinic flux spectroradiometry: A

technique for measuring photolysis frequencies in the atmosphere, APPLIED OPTICS, 38, 4443–4460, 10.1364/AO.38.004443, 1999.

Hofzumahaus, A., Lefer, B. L., Monks, P. S., Hall, S. R., Kylling, A., Mayer, B., Shetter, R. E., Junkermann, W., Bais, A., Calvert, J. G., Cantrell, C. A., Madronich, S., Edwards, G. D., Kraus, A.: Photolysis frequency of O_3 to $O(^1D)$: Measurements and modeling during the International Photolysis Frequency Measurement and Modeling Intercomparison (IPMMI), JOURNAL OF GEOPHYSICAL RESEARCH-ATMOSPHERES, 109 (D8), D08S90, 10.1029/2003JD004333, 2004.

Jacobson, M, Z.: Studying the effects of aerosols on vertical photolysis rate coefficient and temperature profiles over an urban airshed, JOURNAL OF GEOPHYSICAL RESEARCH-ATMOSPHERES, 103, 10593–10604, 10.1029/98JD00287, 1998.

Jones, I. T. N. and Bayes, K.D. Photolysis of nitrogen dioxide, J. Chem. Phys. 59, 4836-4844, 1973.

Kazadzis, S., Bais, A. F., Balis, D., Zerefos, C. S., and Blumthaler, M. Retrieval of down-welling UV actinic flux density spectra from spectral measurements of global and direct solar UV irradiance, J. Geophys. Res., 105, 4857-4864, 2000.

Kazadzis, S., Topaloglou, C., Bais, A. F., Blumthaler, M., Balis, D., Kazantzidis, A., Schallhart, B. Actinic flux and O^1D photolysis frequencies retrieved from spectral measurements of irradiance at Thessaloniki, Greece, ATMOSPHERIC CHEMISTRY AND PHYSICS, 4, 2215-2226, DOI: 10.5194/acp-4-2215-2004, 2004.

Kazadzis, S., Amiridis, V., and Kouremeti, N. The Effect of Aerosol Absorption in Solar UV Radiation, Advances in Meteorology, Climatology and Atmospheric Physics, 1041-1047, 2012.

Krotkov, N., Bhartia, P. K., Herman, J., Slusser, J., Scott, G., Labow, G., Vasilkov, A. P., Eck, T. F., Dubovik, O., Holben, B. N. Aerosol ultraviolet absorption experiment (2000 to 2004), part 2: Absorption optical thickness, refractive

index, and single scattering albedo, OPTICAL ENGINEERING, 44, 4, 041005. DOI: 10.1117/1.1886819, 2005.

Kylling, A., Webb, A. R., Bais, A. F., Blumthaler, M., Schmitt, R., Thiel, S., Kazantzidis, A., Kift, R., Misslebeck, M., Schallhart, B., Schreder, J., Topaloglou, C., Kazadzis, S., and Rimmer, J.: Actinic flux determination from measurements of irradiance, J. Geophys. Res., 108 (D16), 4506-4515, 2003.

Lefer, B. L., Shetter, R. E., Hall, S. R.: Impact of clouds and aerosols on photolysis frequencies and photochemistry during TRACE-P: 1. Analysis using radiative transfer and photochemical box models, JOURNAL OF GEOPHYSICAL RESEARCH-ATMOSPHERES, 108, 8821-8835, 10.1029/2002JD003171, 2003.

Li C C, Mao J T, Liu Q H. Using MODIS to study the distribution and seasonal variation of aerosol optical thickness in eastern China. Science Bulletin (China), 48: 2094-2100. 2003.

Li, J., Wang, Z. F., Wang, X., Yamaji, K., Takigawa, M., Kanaya, Y., Pochanart, P., Liu, Y., Irie, H., Hu, B., Tanimoto, H., Akimoto, H.: Impacts of aerosols on summertime tropospheric photolysis frequencies and photochemistry over Central Eastern China, ATMOSPHERIC ENVIRONMENT, 45: 1817-1829, 10.1016/j.atmosenv.2011.01.016, 2011.

Liao, H., Yung, Y. L., and Seinfeld, J. H.: Effects of aerosols on tropospheric photolysis rates in clear and cloudy atmospheres, JOURNAL OF GEOPHYSICAL RESEARCH, 104(D19), 23697–23707, 1999.

Liu, Q.Y., Ma, T. M., Olson, M. R., Liu, Y. J., Zhang, T. T., Wu, Y., Schauer, J. J.: Temporal variations of black carbon during haze and non-haze days in Beijing, SCIENTIFIC REPORTS, 6, 33331, 10.1038/srep33331, 2016.

Lou, S. J; Liao, H; Zhu, B. Impacts of aerosols on surface-layer ozone concentrations in China through heterogeneous reactions and changes in photolysis rates. ATMOSPHERIC ENVIRONMENT, 85:123-138, 0.1016/j.atmosenv.2013.12.004, 2014.

Lu, K. D., Rohrer, F., Holland, F., Fuchs, H., Bohn, B., Brauers, T., Chang, C. C., Häseler, R., Hu, M., Kita, K., Kondo, Y., Li, X., Lou, S. R., Nehr, S., Shao, M., Zeng, L. M., Wahner, A., Zhang, Y. H., Hofzumahaus, A.: Observation and modelling of OH and HO_2 concentrations in the Pearl River Delta 2006: a missing OH source in a VOC rich atmosphere, ATMOSPHERIC CHEMISTRY AND PHYSICS, 12: 1541-1569, 10.5194/acp-12-1541-2012, 2012

Ma, X. Y., Wang, J. Y., Yu, F. Q., Jia, H. L., Hu, Y. N.: Can MODIS AOD be employed to derive PM2.5 in Beijing-Tianjin-Hebei over China? ATMOSPHERIC RESEARCH, 181, 250-256, 10.1016/j.atmosres.2016.06.018, 2016.

Ma, Z. W., Hu, X. F., Huang, L., Bi, J., Liu, Y.: Estimating Ground-Level $PM_{2.5}$ in China Using Satellite Remote Sensing. Environ Sci Technol, 48: 7436−7444.

Madronich, S, The Atmosphere and UV-B Radiation at Ground Level, Environmental UV Photobiology, doi: 0.1007/978-1-4899-2406-3_1. 1993,

Madronich, S., and S. Flocke, The role of solar radiation in atmospheric chemistry, in Environmental Photochemistry, edited by P. Boule, pp. 1-26, Springer-Verlag, New York, 1999.

Mailler, S., Menut, L., di Sarra, A. G., Becagli, S., Di Iorio, T., Bessagnet, B., Briant, R., Formenti, P., Doussin, J. F ., Gomez-Amo, J. L., Mallet, M., Rea, G., Siour, G., Sferlazzo, D. M., Traversi, R., Udisti, R., Turquety, S.: On the radiative impact of aerosols on photolysis rates: comparison of simulations and observations in the Lampedusa island during the ChArMEx/ADRIMED campaign, ATMOSPHERIC CHEMISTRY AND PHYSICS, 16(3):1219-1244, 10.5194/acp-16-1219-2016, 10.5194/acp-16-1219-2016, 2016.

Matsumi, Y., Comes, F.J., Hancock, G., Hofzumahaus, A., Hynes, A.J., Kawasaki, M., Ravishankara, A.R., Quantum yields for production of $O(^1D)$ in the ultraviolet photolysis of ozone: recommendation based on evaluation of laboratory data. Journal of Geophysical Research 107 (D3), 4024. doi:10.1029/2001JD000510. 2002.

892 Malicet, J., Daumont, D., Charbonnier, J., Parisse, C., Chakir, A., Brion, J. Ozone UV
893 spectroscopy. II. Absorption cross-sections and temperature dependence. Journal
894 of Atmospheric Chemistry 21 (3), 263-273, 1995.
895 Peeters, J., Nguyen, T. L., Vereecken, L.: HOX radical regeneration in the oxidation of
896 isoprene. PHYSICAL CHEMISTRY CHEMICAL PHYSICS, 11: 5935-5939,
897 10.1039/b908511d, 2009.
898 Pere, J. C., Bessagnet, B., Pont, V., Mallet, M., Minvielle, F.: Influence of the
899 aerosol solar extinction on photochemistry during the 2010 Russian wildfires
900 episode, ATMOSPHERIC CHEMISTRY AND PHYSICS, 15, 10983-10998,
901 10.5194/acp-15-10983-2015, 2015.
902 Raga, G. B., Castro, T., Baumgardner, D.: The impact of megacity pollution on local
903 climate and implications for the regional environment: Mexico City,
904 ATMOSPHERIC ENVIRONMENT, 35, 1805-1811,
905 10.1016/S1352-2310(00)00275-2, 2001.

906 Real, E. and Sartelet, K.: Modeling of photolysis rates over Europe: impact on
907 chemical gaseous species and aerosols, ATMOSPHERIC CHEMISTRY AND
908 PHYSICS, 11, 1711–1727, 10.5194/acp-11-1711-2011, 2011.
909 Rohrer, F; Lu, K. D; Hofzumahaus, A; Bohn, B ; Brauers, T ; Chang, C. C ; Fuchs,
910 H; Haseler, R; Holland, F; Hu, M., Maximum efficiency in the
911 hydroxyl-radical-based self-cleansing of the troposphere, Nature Geoscience. 7,
912 559-563, 2014.
913 Shetter, R. E., Muller, M.: Photolysis frequency measurements using actinic flux
914 spectroradiometry during PEM-Tropics Mission: Instrumentation description and
915 some results, JOURNAL OF GEOPHYSICAL RESEARCH-ATMOSPHERES,
916 104, 5647-5661, 10.1029/98JD01381, 1999.
917 Shetter, R. E.: Photolysis frequency of NO2: measurement and modeling during the
918 International Photolysis Frequency Measurement and Modeling Intercomparison
919 (IPMMI), JOURNAL OF GEOPHYSICAL RESEARCH-ATMOSPHERES, 108,
920 8544, 10.1029/2002JD002932, 2003.

Stone, D; Whalley, L. K; Heard, D. E. Tropospheric OH and HO_2 radicals: field measurements and model comparisons, Chem. Soc. Rev,41(19): 6348-6404, 10.1039/c2cs35140d, 2012.

Tang, Y., Carmichael, G. R., Kurata, G., Uno, I., Weber, R. J., Song, C. H., Guttikunda, S. K., Woo, J. H., Streets, D. G., Wei, C., Clarke, A. D., Huebert, B., Anderson, T. L.: Impacts of dust on regional tropospheric chemistry during the ACE-Asia experiment: a model study with observations, JOURNAL OF GEOPHYSICAL RESEARCH-ATMOSPHERES, 109, D19S21, 10.1029/2003JD003806, 2004.

Tian, P., Wang, G. F., Zhang, R. J., Wu, Y. F., Yan, P.: Impacts of aerosol chemical compositions on optical properties in urban Beijing, China, PARTICUOLOGY, 18, 155-164, 10.1016/j.partic.2014.03.014, 2015.

Tie, X. X., Madronich, S., Walters, S., Edwards, D. P., Ginoux, P., Mahowald, N., Zhang, R. Y., Lou, C., Brasseur, G.: Assessment of the global impact of aerosols on tropospheric oxidants. JOURNAL OF GEOPHYSICAL RESEARCH-ATMOSPHERES, 110, D03204, 10.1029/2004JD005359, 2005.

Topaloglou, C., Kazadzis, S., Bais, AF., Blumthaler, M., Schallhart, B., Balis, D. NO_2 and HCHO photolysis frequencies from irradiance measurements in Thessaloniki, Greece. ATMOSPHERIC CHEMISTRY AND PHYSICS, 5, 1645-1653, DOI: 10.5194/acp-5-1645-2005, 2005.

Trebs, I., Bohn, B., Ammann, C., Rummel, U., Blumthaler, M., Konigstedt, R., Meixner, F. X ., Fan, S., Andreae, M. O. Relationship between the NO 2 photolysis frequency and the solar global irradiance, ATMOSPHERIC MEASUREMENT TECHNIQUES, 2, 725-739, DOI: 10.5194/amt-2-725-2009, 2009.

van Donkelaar, A., Martin, R. V., Brauer, M., Kahn, R., Levy, R., Verduzco, C., and Villeneuve, P. J.: Global Estimates of Ambient Fine Particulate Matter Concentrations from Satellite-Based Aerosol Optical Depth: Development and Application. Environmental Health Perspectives, 118, 847-855, 10.1289/ehp.0901623, 2010.

950 Verstraeten, W, W., Neu, J. L., Williams, J. E., Bowman, K. W., Worden, J. R.,
951 Boersma, K. F.: Rapid increases in tropospheric ozone production and export
952 from China. NATURE GEOSCIENCE, 8, 690-695, 10.1038/NGEO2493, 2015.
953 Volkamer R, Sheehy P, Molina L T, Molina M J.: Oxidative capacity of the Mexico
954 City atmosphere – Part 1: A radical source perspective, ATMOSPHERIC
955 CHEMISTRY AND PHYSICS, 10, 6969–6991, 10.5194/acp-10-6969-2010,
956 2010.
957 Wang, B.,Shao, M., Lu, S. H., Yuan, B., Zhao, Y., Wang, M., Zhang, S. Q., Wu, D.:
958 Variation of ambient non-methane hydrocarbons in Beijing city in summer 2008,
959 ATMOSPHERIC CHEMISTRY AND PHYSICS, 10, 5911–5923,
960 10.5194/acp-10-5911-2010, 2010.
961 Wang, Q., Sun, Y., Jiang, Q., Du, W., Sun, C., Fu, P., Wang, Z.: Chemical
962 composition of aerosol particles and light extinction apportionment before and
963 during the heating season in Beijing, China. JOURNAL OF GEOPHYSICAL
964 RESEARCH-ATMOSPHERES, 120: 12,708-12,722, 10.1002/2015JD023871,
965 2015.
966 Xin, J. Y; Gong, C. S; Liu, Z. R; Cong, Z. Y; Gao, W. K; Song, T; Pan, Y. P; Sun,
967 Y; Ji, D. S; Wang, L. L; Tang, G. Q; Wang, Y. S.: The observation-based
968 relationships between $PM_{2.5}$ and AOD over China, JOURNAL OF
969 GEOPHYSICAL RESEARCH-ATMOSPHERES, 121, 10701-10716,
970 10.1002/2015JD024655, 2016.
971 Xu, J., Ma, J. Z., Zhang, X. L., Xu, X. B., Xu, X. F., Lin, W. L., Wang, Y., Meng, W.,
972 and Ma, Z. Q.: Measurements of ozone and its precursors in Beijing during
973 summertime: impact of urban plumes on ozone pollution in downwind rural
974 areas, ATMOSPHERIC CHEMISTRY AND PHYSICS, 11, 12241–12252,
975 10.5194/acp-11-12241-2011, 2011.
976 Zhang, J. P., Zhu, T., Zhang, Q. H., Li, C. C., Shu, H. L., Ying, Y., Dai, Z. P., Wang,
977 X., Liu, X. Y., Liang, A. M., Shen, H. X., and Yi, B. Q.: The impact of
978 circulation patterns on regional transport pathways and air quality over Beijing

and its surroundings, ATMOSPHERIC. CHEMISTRY AND PHYSICS, 12, 5031–5053, 10.5194/acp-12-5031-2012, 2012.

Zhang, L.; Shao, J.; Lu, X.; Zhao, Y.; Hu, Y.; Henze, D. K.; Liao, H.; Gong, S.; Zhang, Q.: Sources and Processes Affecting Fine Particulate Matter Pollution over North China: An Adjoint Analysis of the Beijing APEC Period. ENVIRONMENTAL SCIENCE & TECHNOLOGY, 50(16), 8731-8740, 10.1021/acs.est.6b03010, 2016.

Zhang, Q., Yuan, B., Shao, M., Wang, X., Lu, S., Lu, K., Wang, M., Chen, L., Chang, C. C., Liu, S. C.: Variations of ground-level O3 and its precursors in Beijing in summertime between 2005 and 2011, ATMOSPHERIC CHEMISTRY AND PHYSICS, 14, 6089-6101, 10.5194/acp-14-6089-2014, 2014.

Zhang, R., Jing, J., Tao, J., Hsu, S. C., Wang, G., Cao, J., Lee, C. S. L., Zhu, L., Chen, Z., Zhao, Y., Shen, Z.: Chemical characterization and source apportionment of $PM_{2.5}$ in Beijing: seasonal perspective, ATMOSPHERIC CHEMISTRY AND PHYSICS, 13, 7053-7074, 10.5194/acp-13-7053-2013, 2013.

Zheng, C. W., Zhao, C. F., Zhu, Y. N., Wang, Y., Shi, X. Q., Wu, X. L., Chen, T. M., Wu, F., Qiu, Y. M.: Analysis of influential factors for the relationship between $PM_{2.5}$ and AOD in Beijing, ATMOSPHERIC CHEMISTRY AND PHYSICS, 17, 13473-13489, 10.5194/acp-17-13473-2017, 2017.

Table ~~2~~1. O_3 column concentration, temperature, relative humidity, daytime clear-sky fraction and respective standard deviation for different seasons (spring: March, April and May; summer: June, July and August; autumn: September, October and November; winter: December, January and February).

Season	O_3 column (Du)	Temperature (℃)	Relative humidity (%)	Clear-sky fraction(%)
Spring	355±37	16±7.8	33±18	41
Summer	310±24	28±4.2	57±18	36
Autumn	304±23	16±7.4	46±21	42
Winter	347±28	0.53±4.2	30±18	41

Table ~~1~~2. Instruments deployed in the field campaign undertaken in August 2012 and used for data analysis.

Parameters	Measurement technique	Time resolution	Detection limit	Accuracy
$j(O^1D)$ and $j(NO_2)$	Spectroradiometer	10 s	/	± 10%
O_3	UV photometry	60 s	0.5 ppbv	± 5%
NO	Chemiluminescence	60 s	60 pptv	± 20%
NO_2	Chemiluminescence	60 s	300 pptv	± 20%
CO	IR photometry	60 s	4 ppb	± 5%
SO_2	Pulsed UV fluorescence	60 s	0.1 ppbv	± 5%
HCHO	Hantzsch fluorimetry	60 s	25 pptv	± 5%
VOCs	GC-FID/MS	1 h	20-300 pptv	± 15~20%

Table 3. Slope, intercept and the square of correlation coefficient (r^2) of linear fits of correlation between $j(O^1D)$ and AOD for each ozone column class at AOD smaller than 0.7.

	SZA=30°			SZA=60°		
O_3 column (DU)	Slope ($10^{-6}s^{-1}$)	Intercept ($10^{-6}s^{-1}$)	r^2	Slope ($10^{-6}s^{-1}$)	Intercept ($10^{-6}s^{-1}$)	r^2
300-330	-6.2±1.5	26±1	0.34	-4.2±0.4	7.7±0.3	0.41
330-360	-6.5±1.4	23±1	0.40	-5.0±0.3	7.1±0.2	0.52
360-390	-9.5±1.6	21±1	0.52	-6.9±0.6	7.6±0.3	0.66

Table 4. Slope, intercept and the square of correlation coefficient (r^2) of linear fits of correlation between $j(NO_2)$ and AOD for each ozone column class at AOD smaller than 0.7.

cos(SZA)	Slope (10^{-3} s^{-1})	Intercept (10^{-3} s^{-1})	r^2
0-0.2	-1.3±0.1	1.5±0.0	0.52
0.2-0.4	-2.4±0.1	3.4±0.0	0.41
0.4-0.6	-3.2±0.1	5.5±0.0	0.49
0.6-0.8	-2.1±0.1	7.2±0.1	0.38
0.8-1.0	-1.8±0.1	8.1±0.1	0.26

Table 5. The fitting parameters a_1-a_6 and determination coefficients of E5 for $j(NO_2)$.

a_1	a_2	a_3	a_4	a_5	a_6	r^2
		$\times 10^{-3}$				
-0.46 ± 0.05	-2.0 ± 0.03	13± 0.2	0.22± 0.01	0.32± 0.05	-4.0± 0.1	0.96

Table 6. The fitting parameters a_1-a_6 and determination coefficients of ~~E5~~ E6 for $j(O^1D)$ at ozone column range = 300-330 DU.

a_1	a_2	a_3	a_4	a_5	a_6	r^2
		$\times 10^{-6}$				
1.1 ± 0.3	0.58 ± 0.17	-8.7± 0.9	0.63 ± 0.05	-7.5 ± 0.3	43 ± 1	0.96

Table 7. Mean and standard deviation of observed data during daytime (6:00–18:00) for A day and B day.

Observed data	A day: August 21, 2012	B day: August 26, 2012
AOD	0.21 ± 0.05	3.2 ± 0.4
$PM_{2.5}$ ($\mu g\ m^{-3}$)	22 ± 9	125 ± 16
O_3 column (Du)	302 ± 3	301± 3
Temperature(°C)	28 ± 3	28 ± 3
Relative humidity (%)	48 ± 10	55 ± 12
$j(O^1D)(s^{-1})$	$1.6\times 0^{-5} \pm 1.2\times10^{-5}$	$6.9\times10^{-6} \pm 5.2\times10^{-6}$
$j(NO_2)(s^{-1})$	$5.4\times10^{-3} \pm 2.9\times10^{-3}$	$2.9\times10^{-3}\pm 1.7\times10^{-3}$
O_3 (ppb)	40 ± 17	87 ± 53
NO_2 (ppb)	11 ± 5	25± 10
CO (ppm)	0.24 ± 0.05	0.85 ± 0.14
VOC reactivity (s^{-1})	3.0 ± 0.7	6.4 ± 1.7
HCHO (ppb)	2.7± 1.1	7.4± 1.9

Table 8. Monthly mean and standard deviation of observed data during daytime (6:00–18:00) under the condition of AOD less than 1 and larger than 1 in August 2012

Observed data	AOD<1	AOD>1
AOD	0.43 ± 0.24	2.0 ± 0.8
$PM_{2.5}$ ($\mu g\ m^{-3}$)	26 ± 12	77 ± 47
O_3 column (Du)	303 ± 4	302 ± 5
Temperature(°C)	30 ± 4	29 ± 4
Relative humidity (%)	42 ± 16	57± 13
$j(O^1D)(s^{-1})$	$1.6\times10^{-5} \pm 1.1\times10^{-5}$	$1.0\times10^{-5} \pm 0.7\times10^{-5}$
$j(NO_2)(s^{-1})$	$5.6\times10^{-3} \pm 2.4\times10^{-3}$	$3.8\times10^{-3} \pm 1.7\times10^{-3}$
O_3 (ppb)	52 ± 34	68 ± 46
NO_2 (ppb)	16 ± 7.8	24 ± 9
CO (ppm)	0.47 ± 0.20	0.95 ± 0.47
VOC reactivity (s^{-1})	4.3 ± 1.7	6.2 ± 2.2
HCHO (ppb)	4.0 ± 1.4	6.5± 1.9

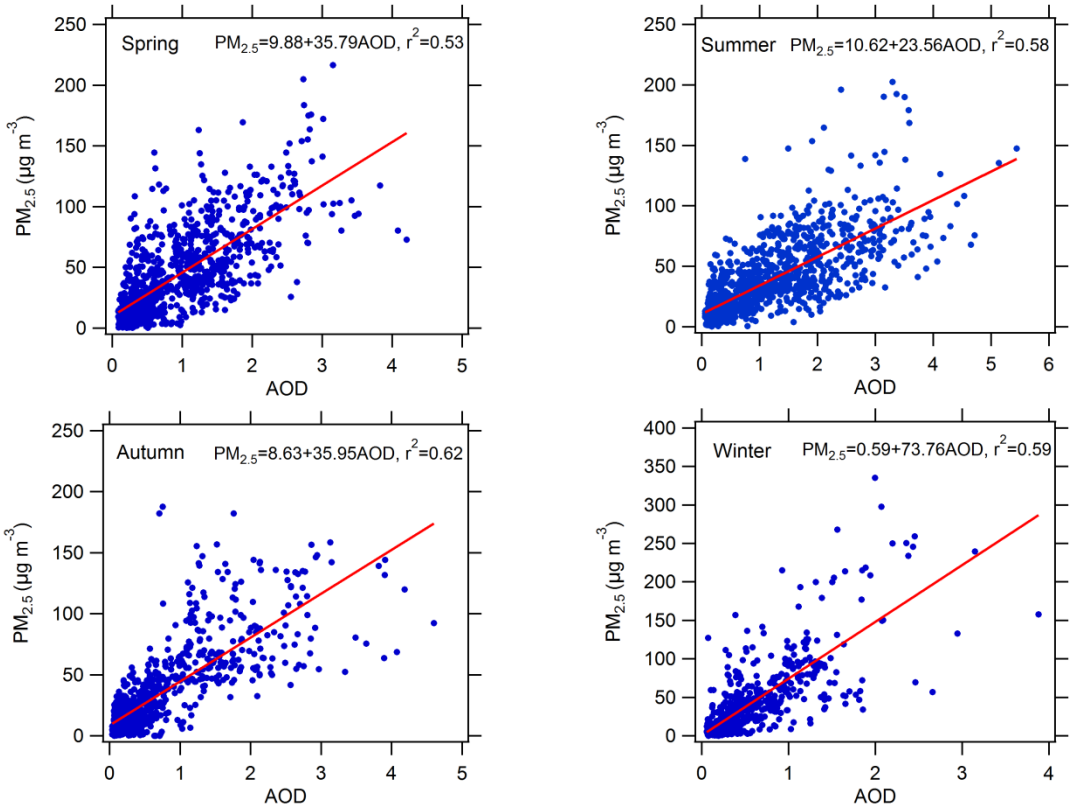

Figure 1. Scatter plots between AOD at 380nm and $PM_{2.5}$ in four different seasons. The slope, intercept and determination coefficient (r^2) were calculated.

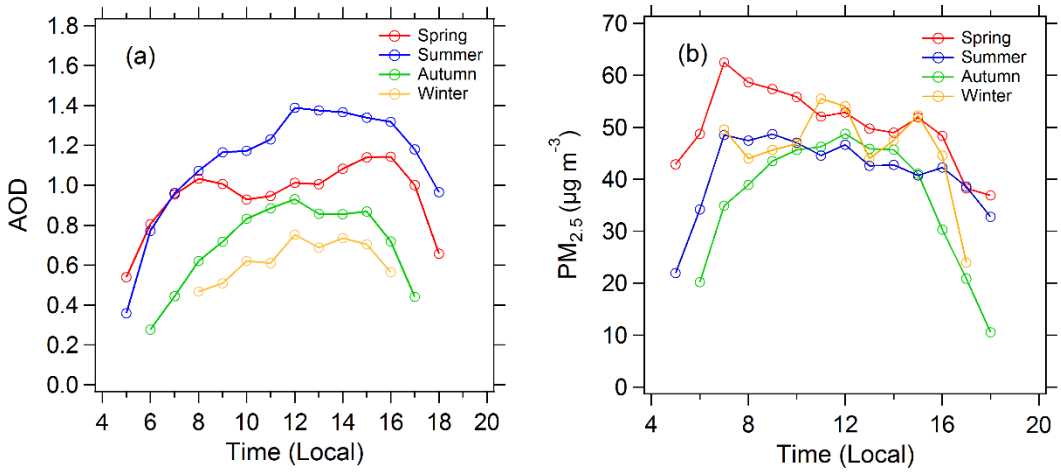

Figure 2. Diurnal cycles of (a) mean AOD and (b) mean $PM_{2.5}$ in the four seasons under cloudless conditions.

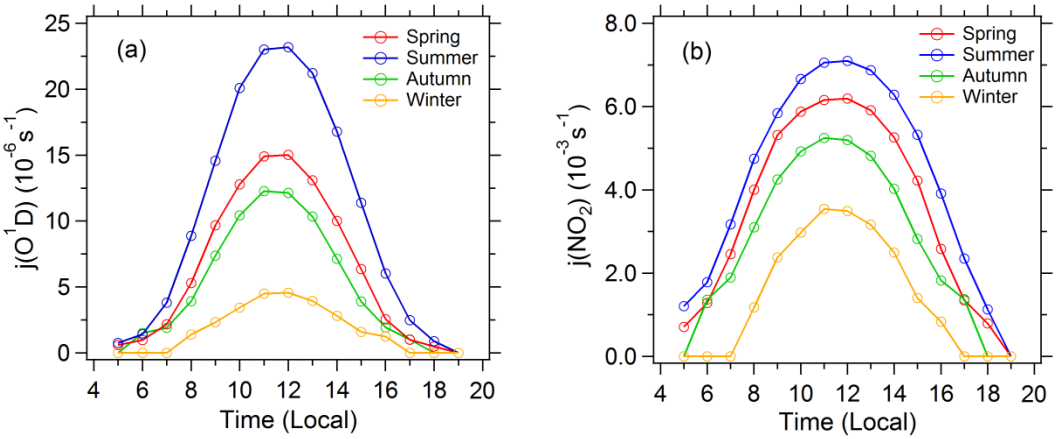

Figure 3. Diurnal cycles of (a) mean $j(O^1D)$ and (b) mean $j(NO_2)$ in the four seasons under cloudless conditions.

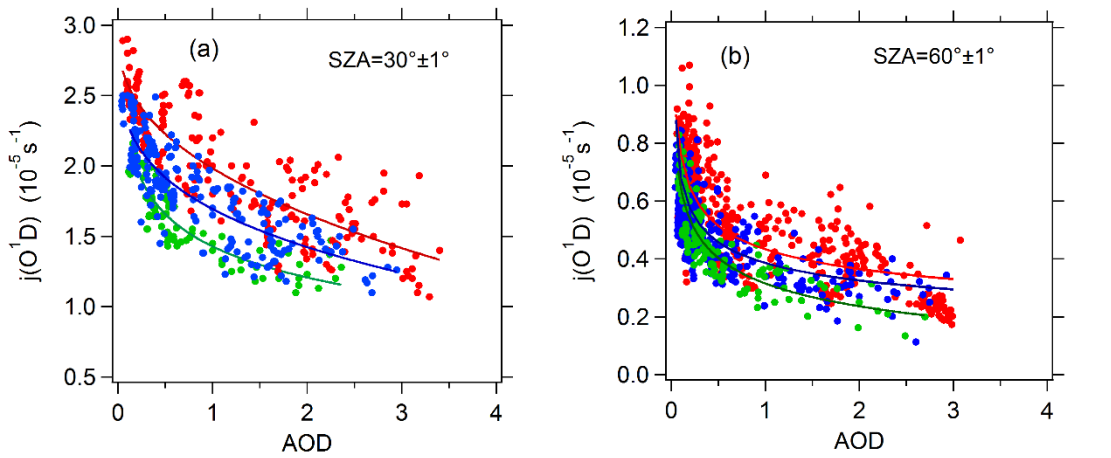

Figure 4. Dependence of $j(O^1D)$ on AOD (380nm) at SZA of (a) 30° and (b) 60° and at different classes of ozone column concentration: 300-330 DU (red), 330-360 DU (blue), and 360-390 DU (green). The full lines are fitted by exponential function.

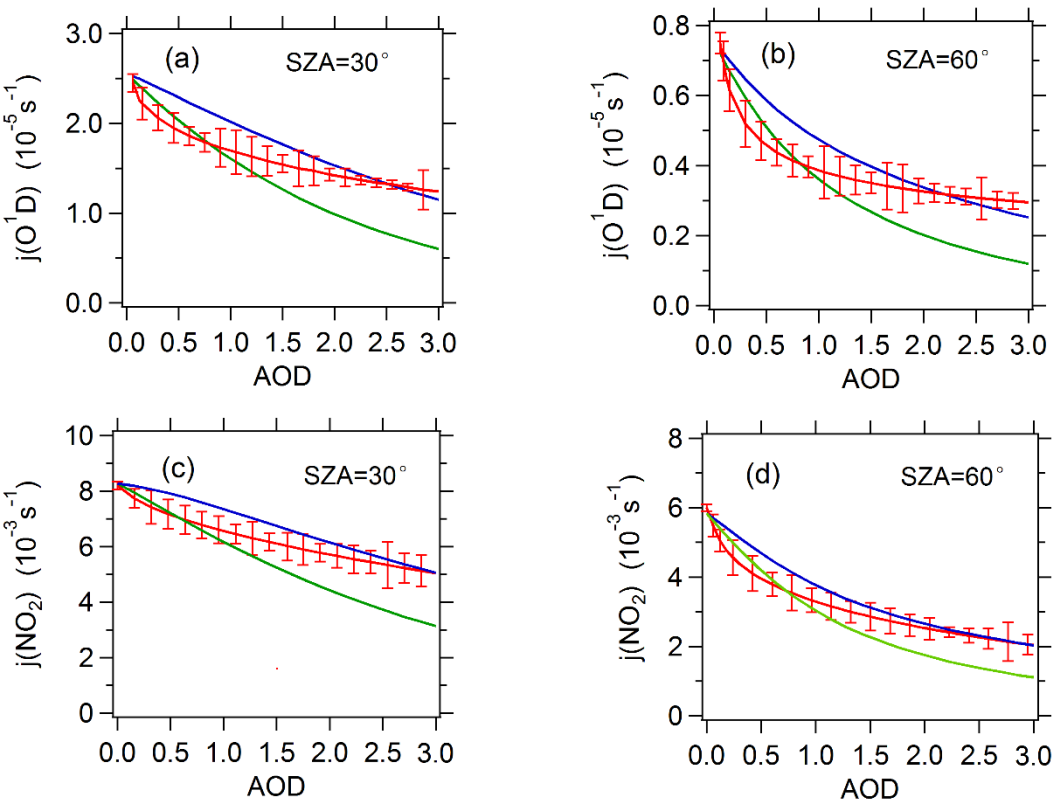

Figure 5. The relationship between observed or TUV-simulated photolysis frequencies and AOD (380nm) at SZA of 30° and 60°. For $j(O^1D)$, total ozone column classification of 330-360 DU is chosen. The red line represents observed average photolysis frequencies; the blue line and green line represents TUV-simulated average photolysis frequencies at SSA of 0.95 and 0.85 respectively.

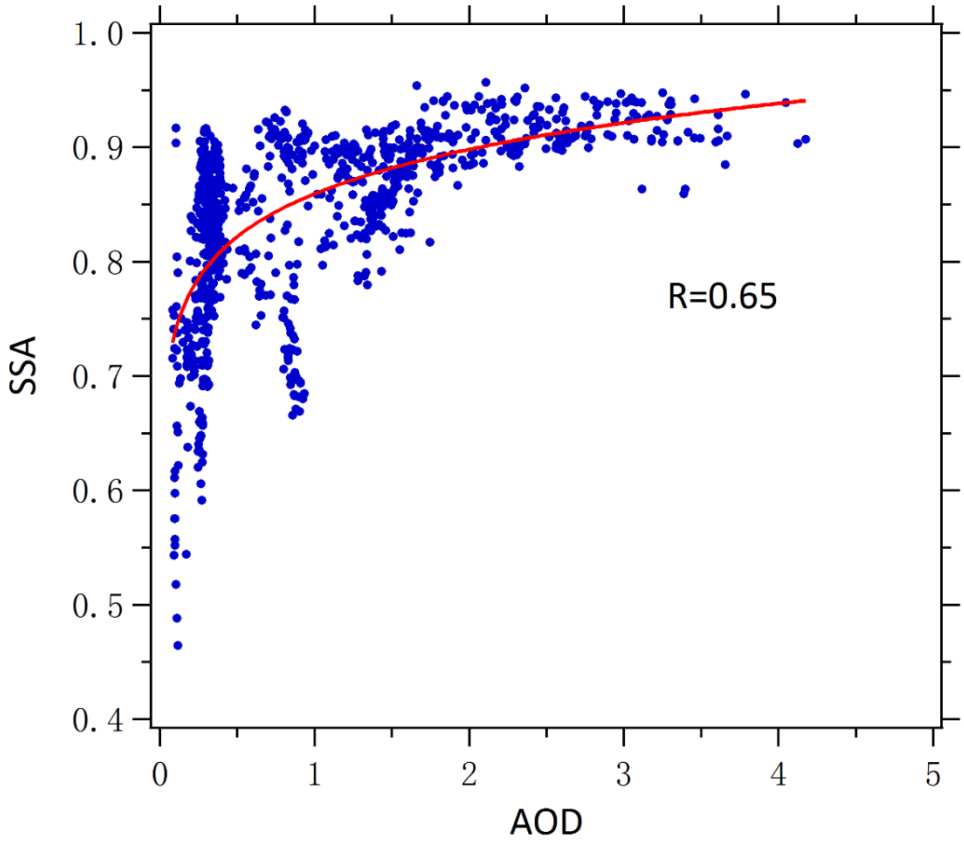

Figure 6. Correlation between SSA and AOD (380nm) observed in August 2012.

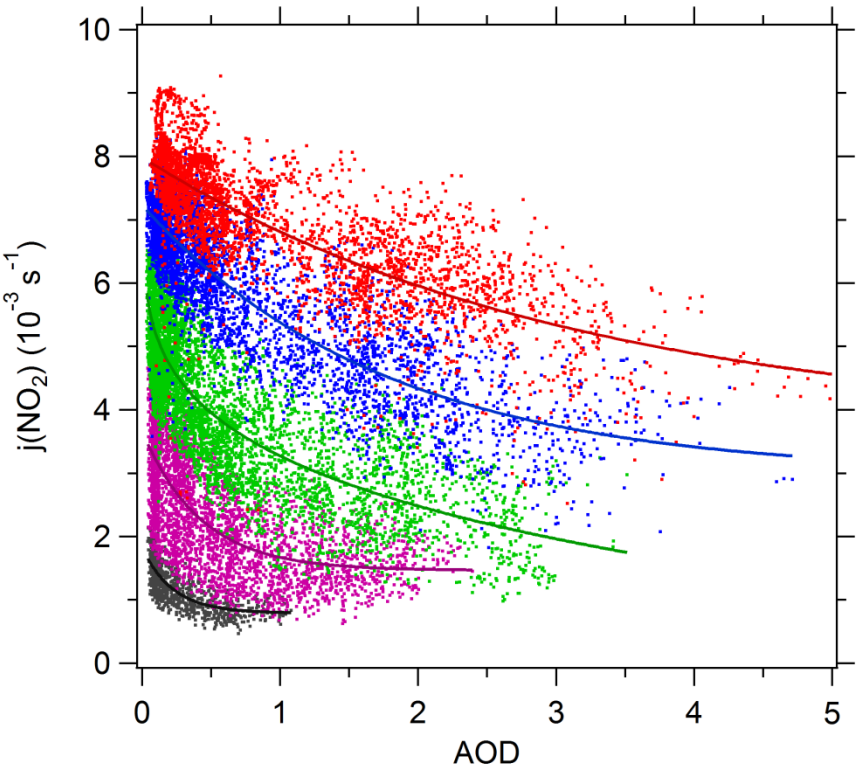

Figure 7. Dependence of $j(NO_2)$ on AOD (380nm) at different SZA classes. The classes of cos(SZA) are 0–0.2 (black), 0.2–0.4 (purple), 0.4–0.6 (green), 0.6–0.8 (blue), and 0.8–1 (red). The full lines are fitted by exponential function.

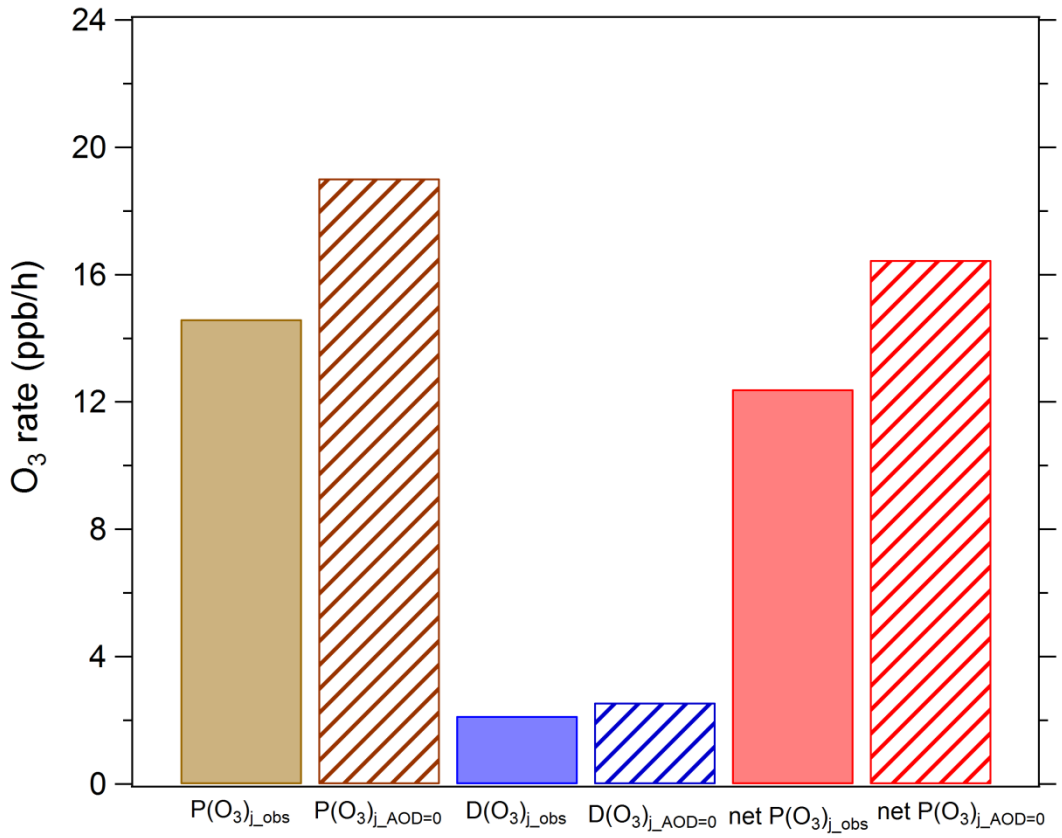

Figure 8. ~~Average~~ Mean daytime ozone production and loss terms in August 2012. $P(O_3)_{j\_obs}$, $D(O_3)_{j\_obs}$ and net $P(O_3)_{j\_obs}$ represents ozone production rate, ozone loss rate, and net ozone production rate under observed photolysis frequencies; $P(O_3)_{j\_AOD=0}$, $D(O_3)_{j\_AOD=0}$ and net $P(O_3)_{j\_AOD=0}$ represents ozone production rate, ozone loss rate, and net ozone production rate under calculated photolysis frequencies when AOD is equal to 0.

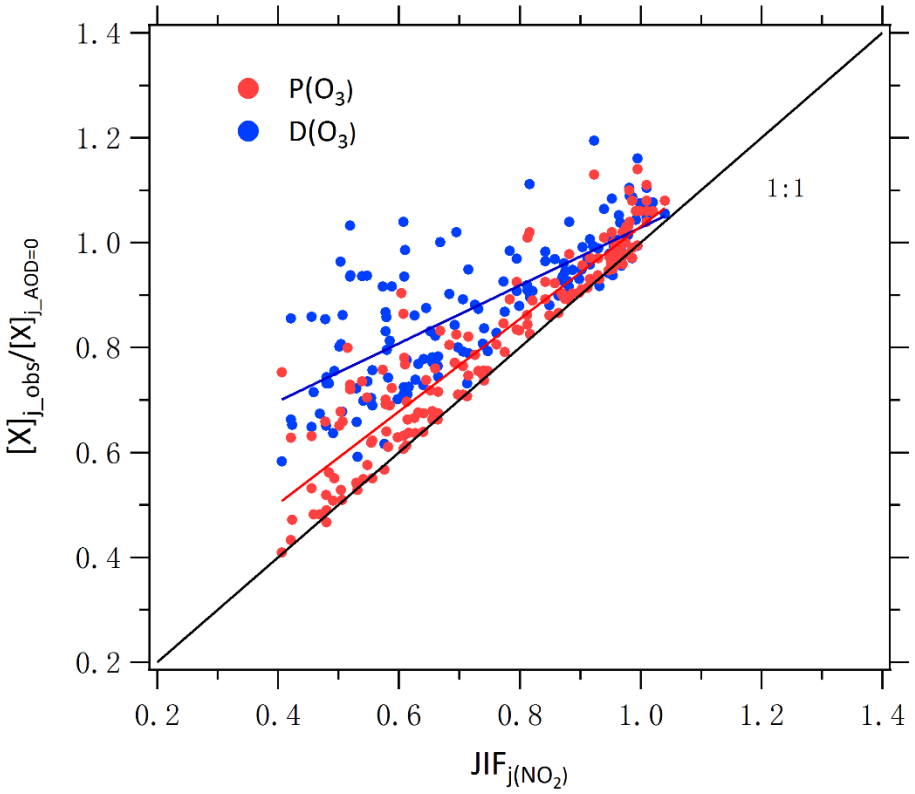

Figure 9. Correlation between $P(O_3)_{j\_obs}/P(O_3)_{j\_AOD=0}$ (or $D(O_3)_{j\_obs}/D(O_3)_{j\_AOD=0}$) and JIF of $j(NO_2)$. Single data point represent daytime hourly mean value.

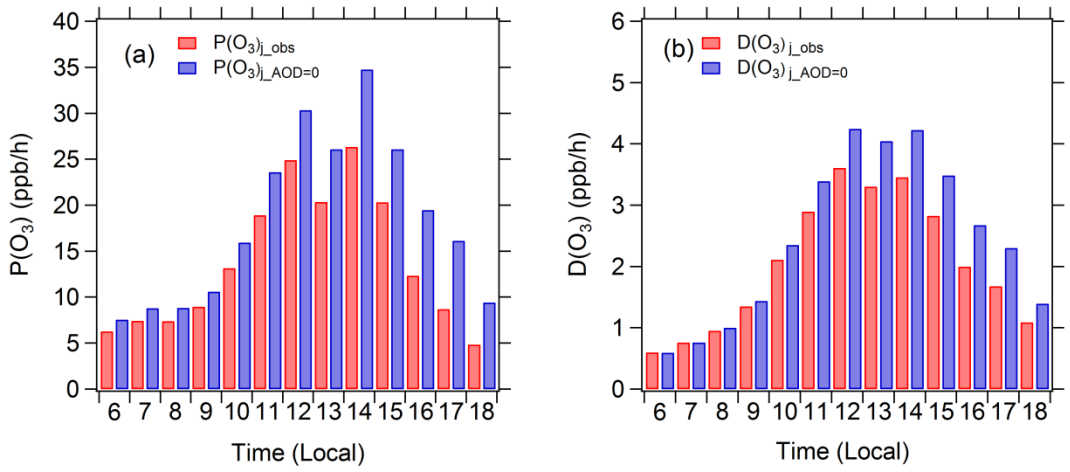

Figure 10. Diurnal profiles of mean $P(O_3)_{j\_obs}$, $P(O_3)_{j\_AOD=0}$, $D(O_3)_{j\_obs}$, and $D(O_3)_{j\_AOD=0}$ in August 2012 under clear-sky conditions.

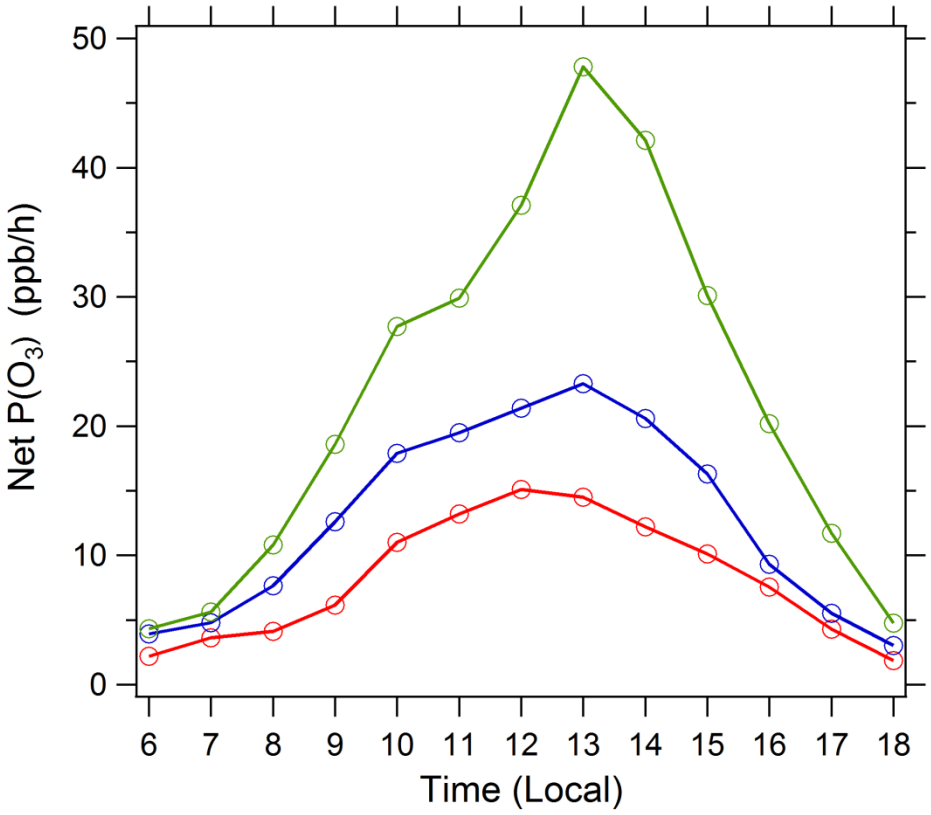

Figure 11. Diurnal profile of net $P(O_3)$ simulated by the box model. Three cases are displayed: (1) A day (red circles): August 21, 2012 with low AOD level and high photolysis frequencies; (2) B day (blue circles): August 26, 2012 with high AOD level and low photolysis frequencies; and (3) the photolysis frequencies of B day adjusted to the level of A day with other conditions unchanged (green circles). The specific conditions of A day and B day are listed in Table 7.

Supporting information

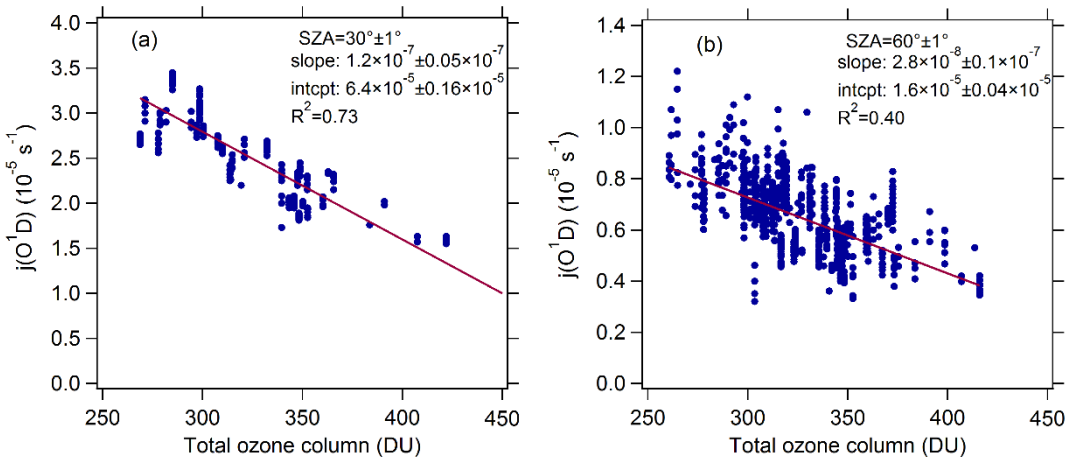

Figure S1. Dependence of $j(O^1D)$ on AOD (380nm) at low AOD level (AOD<0.3) and SZA of (a) 30°±1° and (b) 60°±1°, respectively.

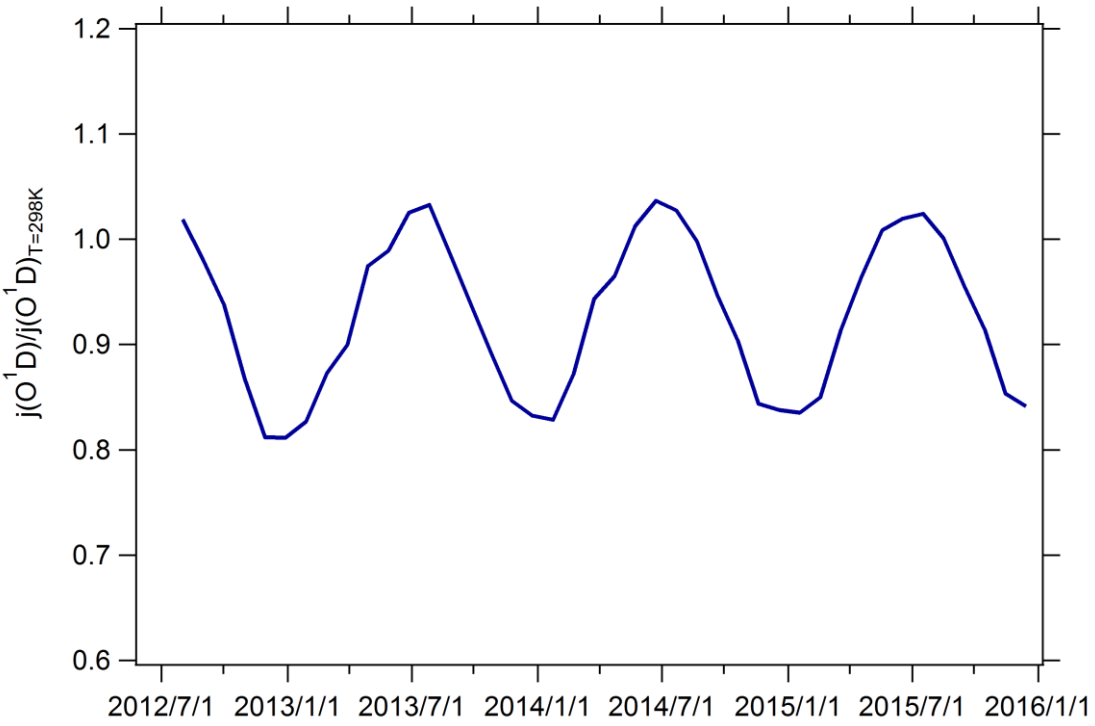

Figure S2. The time series of the monthly mean ratio of $j(O^1D)$ to $j(O^1D)_{T=298K}$ ($j(O^1D)/ j(O^1D)_{T=298K}$) from August 2012 to December 2015.